

Spatial variation, temporal evolution, and source direction apportionment of PM1, PM2.5, and PM10: 3-year assessment in Turin (Po Valley)

*Original*

Spatial variation, temporal evolution, and source direction apportionment of PM1, PM2.5, and PM10: 3-year assessment in Turin (Po Valley) / Mecca, D.; Boanini, C.; Vaccaro, V.; Gallione, D.; Mastromatteo, N.; Clerico, M.. - In: ENVIRONMENTAL MONITORING AND ASSESSMENT. - ISSN 0167-6369. - ELETTRONICO. - 196:1251(2024). [10.1007/s10661-024-13446-9]

*Availability:*

This version is available at: 11583/2995116 since: 2024-12-09T12:14:48Z

*Publisher:*

Springer

*Published*

DOI:10.1007/s10661-024-13446-9

*Terms of use:*

This article is made available under terms and conditions as specified in the corresponding bibliographic description in the repository

*Publisher copyright*

Springer postprint/Author's Accepted Manuscript

This version of the article has been accepted for publication, after peer review (when applicable) and is subject to Springer Nature's AM terms of use, but is not the Version of Record and does not reflect post-acceptance improvements, or any corrections. The Version of Record is available online at: <http://dx.doi.org/10.1007/s10661-024-13446-9>

(Article begins on next page)



# Spatial variation, temporal evolution, and source direction apportionment of PM<sub>1</sub>, PM<sub>2.5</sub>, and PM<sub>10</sub>: 3-year assessment in Turin (Po Valley)

D. Mecca · C. Boanini · V. Vaccaro · D. Gallione · N. Mastromatteo · M. Clerico

Received: 22 April 2024 / Accepted: 16 November 2024  
© The Author(s) 2024

**Abstract** As the population of urban areas is increasing continually, analysis of the particulate concentration dynamics in these areas is crucial. Therefore, this study investigated the temporal and spatial variabilities of PM<sub>1</sub>, PM<sub>2.5</sub>, and PM<sub>10</sub> over the urban area of Turin in the Po Valley, Italy, based on high-resolution data from a monitoring campaign conducted between 2018 and 2021 (including COVID-19 lockdown period). The study also performed a source direction analysis of the urban observation using the conditional bivariate probability function

(CBPF). The results showed substantial differences in PM<sub>10</sub> concentration at background (28–30 µg/m<sup>3</sup>), and traffic stations (36 µg/m<sup>3</sup>). PM<sub>2.5</sub> concentration was highest at traffic stations (24 µg/m<sup>3</sup>). During the day, the highest values occurred at 9:00–11:00 AM, and the lowest concentrations occurred at 4:00–6:00 PM. The concentration peak position changed in a daily bimodal trend with the season. According to the CBPF, the relevant external particulate contributions to the Turin area are from the direction of the Po Valley (N–NE) and the typical direction of Saharan dust transport (S–SW). The present study contributes to scientific understanding by providing information on one of the main European pollutant hot spots and discussing the trends of emerging pollutants, like PM<sub>1</sub>.

**Supplementary Information** The online version contains supplementary material available at <https://doi.org/10.1007/s10661-024-13446-9>.

D. Mecca · C. Boanini · V. Vaccaro · D. Gallione (✉) · N. Mastromatteo · M. Clerico  
Politecnico Di Torino, DIATI – Department of Environment, Land and Infrastructure Engineering, Turin, Italy  
e-mail: davide.gallione@polito.it

D. Mecca  
e-mail: ing.domenicomecca@gmail.com

C. Boanini  
e-mail: chiara.boanini8@gmail.com

V. Vaccaro  
e-mail: vincenzo.vaccaro@polito.it

N. Mastromatteo  
e-mail: nicole.mastromatteo@polito.it

M. Clerico  
e-mail: marina.clerico@polito.it

**Keywords** PM<sub>1</sub> · PM<sub>2.5</sub> · PM<sub>10</sub>

## Introduction

Air pollution, one of the nine planetary boundaries, is becoming a global threat to public health and welfare (Brook et al., 2017; ONU, 2015; Steffen et al., 2015). According to the World Health Organization, air pollution causes 7 million premature deaths worldwide every year, and citizens of urban areas are most affected (Juginović et al., 2011; Kuehn, 2014). Because the population in urban areas will grow by 2050, the air pollution problem will become even more important (Michetti et al., 2022; UN, 2018).

Rapid economic growth has prompted the intensive use of fossil fuels, which has increased particulate concentrations of PM<sub>2.5</sub> (atmospheric fine particles with an aerodynamic diameter less than 2.5 µm) and PM<sub>10</sub> (atmospheric coarse particles with an aerodynamic diameter less than 10 µm), as well as concentrations of gases such as nitrogen dioxide (NO<sub>2</sub>), sulfur dioxide (SO<sub>2</sub>), ozone (O<sub>3</sub>), and greenhouse gases such as carbon dioxide (CO<sub>2</sub>) (Atamaleki et al., 2019; Bastola & Sapkota, 2015). Particulate matter plays an important role in public health, generating negative effects on organs such as the lungs, heart, and brain (Delgado-Saborit et al., 2021; Lipfert, 2018; Yao et al., 2022). It also has a strong influence on climate change, inducing a warming effect through the absorption of solar and infrared radiation (Ramanathan & Carmichael, 2008). High aerosol concentrations in the atmosphere above the limit values can have serious consequences for the environment, climate, and human health (Jung et al., 2019; Mehmood et al., 2021; Qayyum et al., 2021; Ur Rehman et al., 2024).

Understanding how particulate matter varies through space and time in different areas is crucial to accurately evaluating the health risks associated with air pollution (Liu et al., 2022). Most epidemiologic studies of short-term exposure have used daily or hourly variations in concentrations measured at air quality monitoring stations (Atkinson et al., 2016). Such estimates, in combination with forecasting models, can help decision-makers take appropriate actions to mitigate pollutant emissions. Moreover, spatiotemporal assessment of contaminants not yet subject to limitations, such as PM<sub>1</sub>, will support institutions working to define future air quality standards (Chen et al., 2017).

The spatial variation of pollutant concentrations results from a dynamic process dominated by multifaceted interactions between local and global emissions derived from human activities, natural emissions, and transport phenomena (Dias & Tchepel, 2018). Meteorological conditions such as rainfall, humidity, and wind speed also promote spatial variation of emissions (Tian et al., 2020; Zhang et al., 2021). Spatial variation in concentrations is monitored according to the criteria of the European Environment Agency. Air quality measurement stations are classified by the characteristics of the measuring area. Specifically, traffic, urban, and background

stations refer to the different contexts characterizing the location where the measurement takes place (Filigrana et al., 2020). According to the European Directive 2008/50/EC, background measurements refer to a context not influenced mostly by specific sources (such as industries or traffic) but affected by the integrated contribution of all sources. The traffic context refers to locations with a high street density and traffic congestion. The concentrations at these locations are affected strongly by traffic emissions. Finally, the urban context refers to urban areas, in which concentrations are affected by a population high density and residential and work activities.

The temporal variation of pollutants can be evaluated at multiple time scales. Observing the seasonal scale, Hu et al. (2014) and Ma and Jia (2016) found that particulate matter and gaseous pollutant concentrations were higher in winter than in other seasons, with the exception of ozone, which reached a maximum in the summer. According to Chen et al. (2020), investigations of the diurnal patterns of air pollutant concentrations and the differences in days with different emission scenarios have crucial importance. They facilitate understanding of specific emission sources and pollutant formation mechanisms. Specifically, workdays and weekend days are generally affected by different pollutant concentrations because they are characterized by different traffic activity. Therefore, by disaggregating the high-resolution data, it is possible to understand the contribution of traffic to pollutant concentrations (Lonati et al., 2006). Batterman et al. (2015) and Zhang et al. (2016) both emphasize the importance of high-resolution data in understanding the spatial and temporal patterns of traffic-related air pollutants.

The combination of inter-site concentration differences and temporal variations is often used by researchers to identify the contribution of different sources based on a receptor approach (Li et al., 2017a, b). Several studies have approached analysis in different continents, including Europe (Chen et al., 2020; Galindo et al., 2018; Lonati et al., 2011) Asia (Kuerban et al., 2020; Zhao et al., 2018), and North America (Chang et al., 2015; Filigrana et al., 2020) and at the city level (Giugliano et al., 2005), regional level (Galindo et al., 2018), and country level (Fan et al., 2020). Despite several studies having performed such analyses in the Po Valley, Italy (Gilar-doni et al., 2020; Giugliano et al., 2005; Lonati et al.,

2011; Tositti et al., 2014), no study has focused on the urban area of Turin.

The present study focused on the Po Valley, with special attention to the metropolitan area of Turin. The Po Valley is one of the most important pollution hot spots in Europe (Gilardoni et al., 2020; Trivelli et al., 2021). This region includes 40% of the population of Italy, is densely industrialized, and produces 50% of the national GDP (Bozzola & Swanson, 2014). Because of the emission intensity and orography of the valley, which is bounded by the Alps to the north and the Apennines to the south, the Po Valley of northern Italy is typically subjected to atmospheric subsidence, which facilitates stagnation of contaminants (Bo et al., 2020; Caserini et al., 2017; Pecorari et al., 2013). In metropolitan areas such as Turin, the second-largest city in Italy, the main problems are attributable to particulate matter concentrations. The legal limits of annual mean  $PM_{10}$  and  $PM_{2.5}$  and the number of high-pollution days are systematically exceeded. To reduce the impacts of acute pollution, traffic restrictions are usually adopted (Invernizzi et al., 2011).

The national lockdown in Italy was imposed from March 10, 2020, to May 17, 2020, with some disparities in the restrictions enforced during this period (Conte et al., 2023). Many international borders were closed, and lockdown restrictions affected millions of people, leading to reduced transport and changing energy consumption patterns (Campanelli et al., 2021). While the agricultural sector remained unaffected by the restrictions of the lockdown legal directives (Granella et al., 2024).

The particularities of air pollution in the Po Valley can be attributed to the interplay of lockdown-induced changes and (Campanelli et al., 2021) identified four different types of medium- and long-range transport events over Italy: fire plumes from Eastern Europe and Montenegro, dust from the Caspian area and the Sahara Desert, and pollution from the Po Valley. These events were found to affect  $PM_{10}$ ,  $PM_{2.5}$ , and  $NO_2$  concentrations, as well as aerosol optical depth (AOD).

The PM concentration, although reduced, remains within the variability of previous years (2016–2019), with a time trend that does not follow the gas trend. These data once again highlight the complex dynamics of PM and the relationships between emissions precursors and the transport, diffusion, and

physico-chemical processes that determine the formation of secondary PM, which constitutes a significant part (in the order of 70%) of  $PM_{10}$  in the Po basin (Deserti et al., 2020). The concentration of  $PM_{10}$  showed a slight reduction in 2016–2019 (Deserti et al., 2020). Diémoz et al. (2021) state that the lockdown effect is discernible both in the early confinement phase and in late 2020 with a 9% increase in  $PM_{2.5}$ , and a 12% decrease in  $PM_{10}$ , relative to average conditions from 2015–2019.

The smaller decrease in  $PM_{10}$  emissions in Po Valley is mainly attributable to heating sources (Deserti et al., 2020) and agricultural activities (Granella et al., 2024).

The data in this paper are consistent with the studies cited so far. Graphs comparing the measured concentrations in the spring period of 2019 (pre-lockdown) and 2020 (lockdown) are given in the supplementary material section. The graphs show that there are no significant variations in  $PM_{2.5}$  concentrations and the monthly average graph for  $PM_{10}$  concentrations indicates slightly higher concentrations in 2020 compared to 2019.

The purpose of this research was to perform a spatial and temporal investigation of atmospheric particulate concentrations ( $PM_1$ ,  $PM_{2.5}$ , and  $PM_{10}$ ) in the metropolitan area of Turin, one of the most critical European sites for air quality problems. Based on an analysis of a long-term dataset of urban observations, the study evaluated the spatiotemporal variations of concentrations of  $PM_1$ ,  $PM_{2.5}$ , and  $PM_{10}$ . Annual, seasonal, monthly, and daily variations of pollutants, hourly patterns of concentrations, and the differences between weekdays and weekends were assessed. Finally, a source direction analysis of urban observations was conducted. The effects of local emissions and global dust transport were investigated by applying two statistical models considering particulate concentrations and wind speed and direction.

## Methods

### Study area

Turin, with a population of approximately 850,000 inhabitants in the city center and more than 1.8 million including the hinterland, is one of the largest cities in Italy. The Turin area is a strategic

point for spatiotemporal evaluation of particulate concentrations because it is one of the main centers of the Po Valley megacity, a known hotspot for atmospheric pollution (Finardi et al., 2014). The Po Valley includes approximately 15 million residents and has an area of approximately 47,800 km<sup>2</sup>. It is bounded by the Alpine chain to the north and the Apennine chain to the south. It is cleansed by the Adriatic Sea to the east.

The Po Valley deserves special research attention because of its unique climatological circumstances. It is characterized by sea, mountains, and valleys and is influenced by Mediterranean and Alpine climates, with rare Saharan contributions (Finardi et al., 2014; Perrone et al., 2012). Turin makes a significant contribution to the pollution of the Po Valley; however, it also suffers the effects of being at the lowest levels of the Po Valley (Bo et al., 2020). Furthermore, its orographic context also holds scientific interest. Turin is exposed to the Po Valley in two directions and is surrounded by hilly relief on one side and the Alpine chain on the other. This setting affects the city's atmospheric stability, which in winter contributes to the high number of pollution events (Pernigotti et al., 2012).

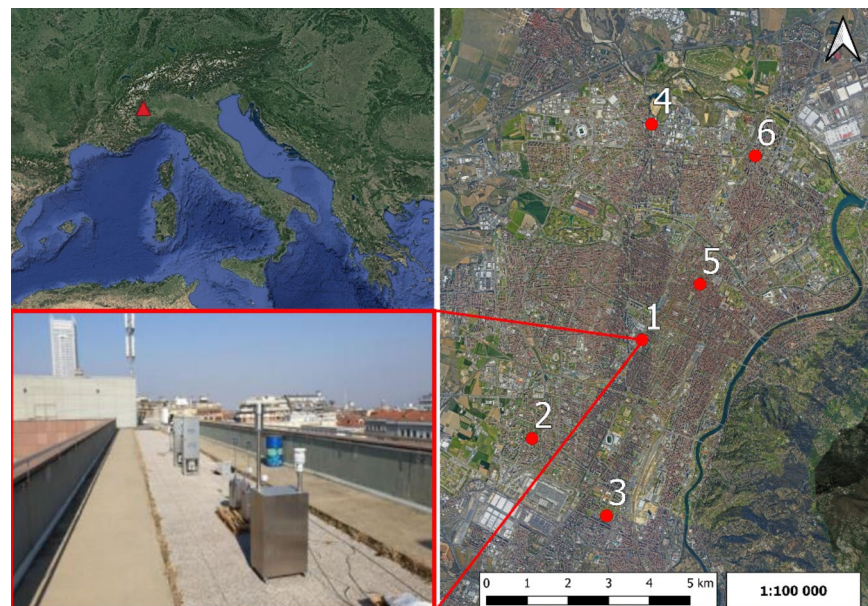
## Measurement instruments

This study was based on observations of particulate matter concentrations at six stations located in the urban area of Turin. Five of the stations belonged to the monitoring network of the public environmental agency, and one was located at the University of Turin Polytechnic (Fig. 1).

The monitoring stations of the public agency provide measurements of particulate matter PM<sub>10</sub> and PM<sub>2.5</sub>. All these stations refer to ZONE IT 0118 and are identified as “urban agglomeration” stations according to the Public Agency characterization. In particular, Rubino Station 2 and Lingotto Station 3 are classified as “background” while Grassi Station 4, Consolata Station 5, and Rebaudengo Station 6 are classified as “traffic,” as the regional environmental agency defines.

This study did not consider industrial stations because they are intended to monitor specific sites affected by local emissions. Further information about the stations is listed in the table in the Supplementary Materials. The data provided by the regional agency for the protection of the environment are available on the web (<https://aria.ambiente.piemonte.it/#/>). Each station includes instruments for measuring particulate concentrations and meteorological conditions. The data from the station located at the University of Turin Polytechnic (Station 1, Politecnico) were

**Fig. 1** Location of measurement sites in the Po Valley and the city of Turin, respectively. The Polytechnic measurement station is depicted in the lower-left illustration



comparable to urban “background” measurements, according to the European directive 2008/50/CE. This station is approximately 24 m above road level, and the measurement site is not affected by adjacent buildings. No commercial or industrial activity takes place on campus. On one side, there is a tree-lined roadway at a sufficient distance. The instrument probes are at a distance from the ground greater than 1.5 m and are spaced from each other according to manual specifications to avoid mutual interference. The following describes the instruments for particulate matter concentrations and meteorological monitoring of Station 1, Politecnico. The Davis Vantage Pro2 (Davis Instruments, Hayward, CA, USA) weather station provided pressure, temperature, relative humidity, wind direction and speed, rain intensity, solar radiation, and UV index data with an acquisition frequency of 1 min. The weather station acquires wind speed within a range from 0 to 89 m/s, with a precision of 0.4 m/s. The wind direction is measured with a range from 1 to 360°, with 1° precision. The particulate matter measurement is by two optical analyzers: an APM-2 (Comde-Derenda GmbH, Stahnsdorf, Germany) and Palas Fidas 200S (Palas GmbH, Karlsruhe, Germany). Both analyzers exploit the Rayleigh scattering principle. Particles entering the analyzer are struck by a visible light beam, with a wavelength of 650 nm in the case of the APM-2 analyzer and multi-wavelengths for the Palas Fidas analyzer. The light scatters on the particles’ surface and the recorded signal are converted into concentration data. More detailed descriptions of the instruments used are available in (Boanini et al., 2021).

#### Quality assurance and control

Quality assurance and quality control (QA/QC) procedures were performed periodically for data certification. The instruments were tested and calibrated periodically according to the operating manual and following the linear regression analysis method, with a slope of  $1 \pm 0.1$ , intercept of  $0 \pm 5 \mu\text{g}/\text{m}^3$ , and correlation coefficient between two groups of data larger than 0.95. In addition, a MicroPNS LVS16 gravity sampler (Umwelttechnik MCZ GmbH, Bad Nauheim, Germany) with 47-mm membranes installed at each measuring station was used to double-check the data. Reasons for anomalously higher concentrations of specific pollutants were identified, and high values

of unknown causes were not discarded randomly. Additionally, the accuracy, logic, comparability, and rationality of the data were checked based on factors such as sampling location and comparisons with historical data series and other station data of the public agency. As required by 2008/50/CE, hourly data were computed only when the sampling time was longer than 45 min in each hour. Each annual period of analysis had at least 324 daily mean concentrations. Furthermore, at least 25 daily mean concentrations were required to calculate monthly average concentrations of the particulate fractions. The data of this study covered the 3 years from September 2018 to September 2021. The time coverage of the data of each station was in the range of 87.9 to 97.4%, and this indicates the amount of data available in the time interval established above. For five of the six stations, the time coverage was greater than the 2008/50/CE threshold limit, which is set at 90%. There were no significant or continuous interruptions in the time series data. Missing data were randomly distributed through the 3 years. Data absence was often due to the shutdown of the control units for maintenance or invalid data.

#### Data acquisition and processing

The APM2 instrument measured the concentrations of  $\text{PM}_{2.5}$  and  $\text{PM}_{10}$  with a time resolution of 2 min. The Palas Fidas instrument measured the values of  $\text{PM}_1$ ,  $\text{PM}_{2.5}$ ,  $\text{PM}_4$ ,  $\text{PM}_{10}$ , PTS, numerical concentration, and dimensional distribution with 1-min time resolution. The high resolution of the data acquisition allowed consideration of both daily and hourly trends. These station data represent the period from September 18, 2018, to September 17, 2021. All data were processed on an hourly basis. The seasonal, weekly, and daily variability of  $\text{PM}_1$ ,  $\text{PM}_{2.5}$ , and  $\text{PM}_{10}$  concentrations and their ratios were studied. For comparisons with public agency monitoring stations, only  $\text{PM}_{10}$  and  $\text{PM}_{2.5}$  are examined since  $\text{PM}_1$  is only available on the University of Turin Polytechnic site. Lastly, a study of hourly trends throughout the day was performed to verify the influence of traffic and planetary boundary layer height (PBLH) on concentrations. The data were processed through Python coding for pre-processing and quality control and for grouping according to temporal and spatial items. Moreover, R coding was used to perform test

statistics and carry out conditional probability function (CPF) and bivariate conditional probability function (CPBF) modeling.

#### Data analysis for CPF and CPBF

To compute CPF and CPBF, wind speed and the wind direction data recorded by the Davis Vantage Pro 2 weather station were used. Wind speed and wind direction were checked by the station every 2.5 s and averaged every minute. For comparison with the hourly concentration data, the wind data were averaged with hourly frequency.

According to Tiwari et al. (2017) assessing the PM concentration with wind direction highlights the contributions of local and global emissions such as combustion from industries, biofuel burning, vehicular emissions, and dust transportation along plains. To do this, statistical tools such as the CPF and CPBF are used. Such models were introduced by Ashbaugh et al. (1985) and Kim et al. (2003) and applied in different contexts by Heo et al. (2009), Squizzato and Masiol (2015), and Tiwari et al. (2014). With the CPF tool, the probability of exceeding a limit value is evaluated for each direction to identify preferential transport directions. The CBPF was applied as an implementation of the CPF (Jain et al., 2020; Tiwari et al., 2017). In this configuration, wind speed is added to the system as an additional variable. The probabilistic relationships combined with wind speed and direction are then utilized to deepen understanding of the spatial distribution of sources.

The CPF statistical model is based on the following formula:

$$CPF_{\Delta\theta} = \frac{\uparrow_{\Delta\theta|c \geq x}}{\eta_{\Delta\theta}} \quad (1)$$

According to this formula, for each angular sector  $\Delta\theta$ , the CPF is equal to the ratio between the occurrences  $m$  of concentration greater than a limit value  $x$  and the number of overall values in the interval  $n$ . From a methodological point of view, 16 angular sectors with an amplitude of  $22.5^\circ$  were selected. For the calculation of probabilities, all concentration values corresponding to a wind speed lower than 0.5 m/s were excluded (Tiwari et al., 2017). This was done because low wind speeds typically have isotropic characteristics of direction (Ashbaugh et al., 1985).

The selected concentration limit value corresponded to the 75th percentile: 22, 26, and  $37 \mu\text{g}/\text{m}^3$  for  $\text{PM}_{10}$ ,  $\text{PM}_{2.5}$ , and  $\text{PM}_{10}$ , respectively.

To perform the CBPF statistical model, the relationship is as follows:

$$CBPF_{\Delta\theta, \Delta u} = \frac{m_{\Delta\theta, \Delta u|y \geq c \geq x}}{n_{\Delta\theta, \Delta u}} \quad (2)$$

For each combination of  $\Delta\theta$  and  $\Delta u$  intervals, the CBPF is equal to the ratio between the occurrences  $m$  of the concentration between the  $y$  and  $x$  limit values and the overall values  $n$  in the interval.

As suggested by Rai et al. (2016) and Uria-Tellaetxe and Carslaw (2014), four concentration ranges (the four main quartiles, 1–25%, 25–50%, 50–75%, and 75–99%) were selected for  $\text{PM}_{10}$ ,  $\text{PM}_{2.5}$ , and  $\text{PM}_{10}$ . To exclude outliers, the extreme percentiles were not considered in the analysis (Uria-Tellaetxe & Carslaw, 2014).

## Results and discussion

### Spatial distribution

Figure 2 shows the  $\text{PM}_{2.5}$  and  $\text{PM}_{10}$  mean concentrations across the 3 years at the monitoring stations. All of the stations measured  $\text{PM}_{10}$ , but only four stations monitored  $\text{PM}_{2.5}$ . The interannual trend of  $\text{PM}_{2.5}$  was similar at the Politecnico, Rubino, and Rebaudengo stations. However, the Lingotto station showed a persistent decreasing trend. The concentrations at the Rebaudengo site were higher than those of the other stations. Unlike the other stations, Rebaudengo is a traffic monitoring station, adjacent to intensely busy urban streets. Its average concentration was highest at 31.56% in the first year, 12.39% in the second year, and 11.65% in the third year.

Among the six stations that measured  $\text{PM}_{10}$  concentrations, the trends at the Grassi and Rebaudengo stations, both traffic stations, over the 3 years were similar. A progressive reduction in concentration occurred. The Politecnico, Rubino, and Lingotto stations showed similar trends of second-year concentrations lower than the concentrations of the other 2 years. The Consolata station had an increasing trend, with a peak in the second year.

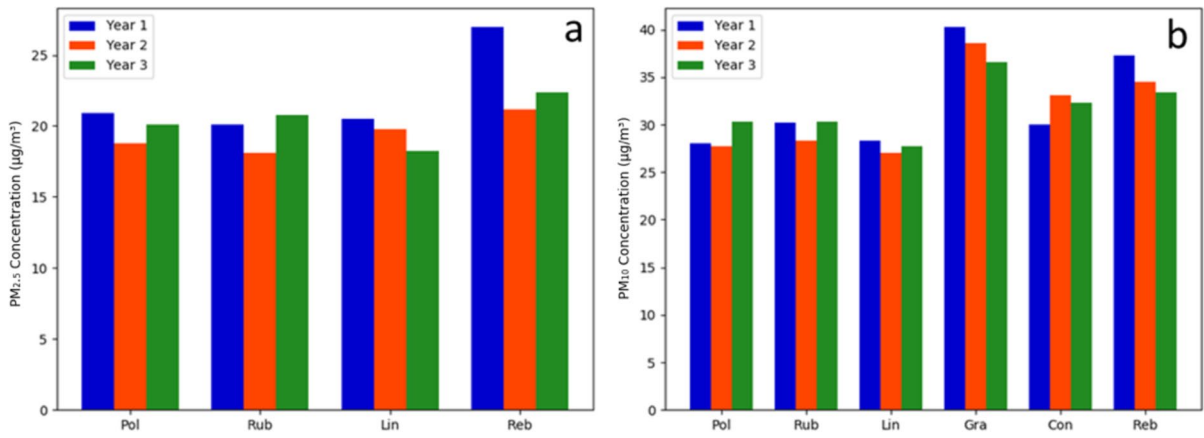


**Fig. 2** a  $PM_{2.5}$  and b  $PM_{10}$  concentrations at the Turin stations during the 3-year period: Year 1 (Sept 2018–Sept 2019), Year 2 (Sept 2019–Sept 2020), and Year 3 (Sept 2020–Sept 2021)

To analyze the spatial differences in concentrations more effectively, a descriptive statistical analysis using box plots is shown in Fig. 3.

Overall, the 3-year mean  $PM_{2.5}$  concentrations were  $20 \mu\text{g}/\text{m}^3$  at Politecnico,  $10 \mu\text{g}/\text{m}^3$  at Rubino,  $20 \mu\text{g}/\text{m}^3$  at Lingotto, and  $24 \mu\text{g}/\text{m}^3$  at the Rebaudengo station. Although the Kruskal–Wallis test suggests a significant difference between concentrations among different measurement points ( $\chi^2_{(3)} = 84.09$ ;  $p < 0.001$ ), the pairwise comparisons using the Mann–Whitney test underlined that only the Rebaudengo concentration was significantly higher than other station ( $p < 0.000$ ), while

no difference was found between Politecnico, Rubino and Lingotto stations ( $p > 0.1$ ).

All monitoring points had a mean lower than the annual limit,  $25 \mu\text{g}/\text{m}^3$  according to 2008/50/EC. The box plots in Fig. 3 show similarities between the Politecnico and Lingotto stations, both background stations, in quartiles and upper and lower limits. However, the Rebaudengo station had a 3-year mean close to the legal limit. Its box plot reveals higher concentration levels in both means and quartiles than at the other stations.

The  $PM_{10}$  concentrations of Politecnico Station 1, Rubino Station 2, Lingotto Station 3, and Consolata Station 5 were not statistically different mean values

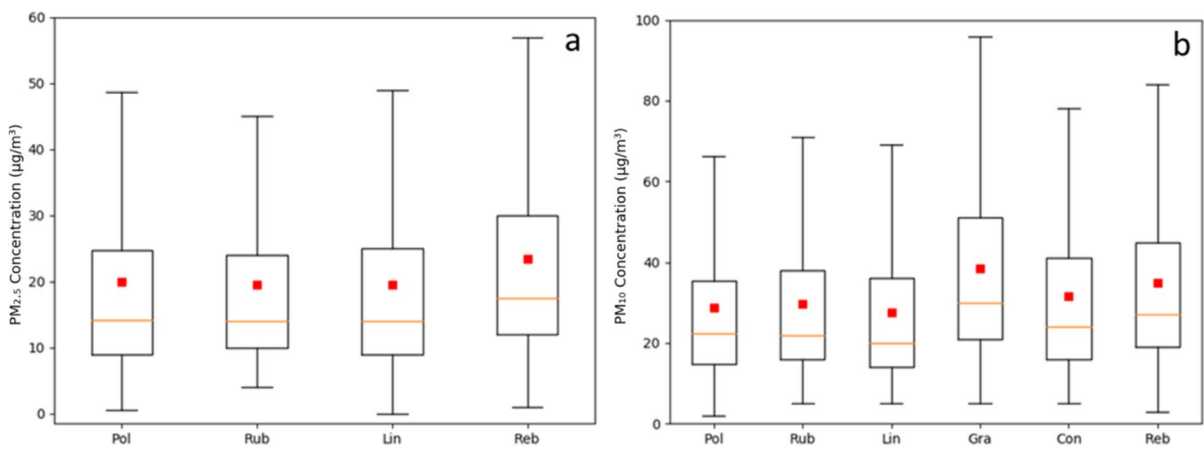


**Fig. 3** Box plot of a  $PM_{2.5}$  and b  $PM_{10}$  concentrations at the Turin stations during Sept 2018 and Sept 2021

equal to  $29 \mu\text{g}/\text{m}^3$  at Politecnico,  $29 \mu\text{g}/\text{m}^3$  at Lingotto ( $z=1.42$ ;  $p>0.05$ ),  $30 \mu\text{g}/\text{m}^3$  at Rubino, and  $31 \mu\text{g}/\text{m}^3$  at Consolata ( $z=1.84$ ;  $p>0.05$ ). Conversely, Grassi station 4 and Rebaudengo station 6 showed significantly different concentration levels ( $z=18.83$ ;  $p<0.001$ ) While the mean at the Grassi station was  $38 \mu\text{g}/\text{m}^3$ , at the Rebaudengo station it was  $34 \mu\text{g}/\text{m}^3$ . Considering box plots in Fig. 3b, the quartiles of these stations were higher positioned than those of the other stations. Although both stations are traffic stations, the Grassi station had higher overall concentrations, because of the different surrounding traffic conditions than at Rebaudengo. Combining the  $\text{PM}_{10}$  concentrations for the same kinds of stations, the Kruskal–Wallis test revealed statistically significant ( $\chi^2_{(2)}=127.4$ ;  $p<0.01$ ) differences among Politecnico and Lingotto ( $29 \mu\text{g}/\text{m}^3$ ), Rubino and Consolata ( $30 \mu\text{g}/\text{m}^3$ ), and Rebaudengo and Grassi ( $36 \mu\text{g}/\text{m}^3$ ) stations. This result confirms the observations of (Boanini et al., 2021; Lonati & Trentini, 2019) about concentrations measured in different spatial contexts.

Concentration distributions for different locations were constructed from the data of the six stations by averaging their daily data (Fig. 4). In this figure are shown curves derived from the data of the six stations: Politecnico and Lingotto in blue, Consolata and Rubino in orange, Rebaudengo and Grassi in green. The frequency distribution was calculated by grouping the data into 20 constant-step classes for  $\text{PM}_{2.5}$  and 24 classes for  $\text{PM}_{10}$ . The size of the classes for both was  $5 \mu\text{g}/\text{m}^3$ .

The concentrations of  $\text{PM}_{2.5}$  and  $\text{PM}_{10}$  showed a left-skewed distribution in all boundary conditions, as also shown by studies carried out at other locations (Fan et al., 2020; Ma & Jia, 2016). The distribution shape is attributable to the impact of the summer period, which is characterized by low concentrations, on the distribution. Furthermore, dilution by rain and wind tends to reduce concentrations, contributing to a high frequency in the lower classes (Ouyang et al., 2015). On the other hand, persistent pollution phenomena and atmospheric stability help to increase the frequency of the higher classes, thus lengthening the tail of the distribution (Galindo et al., 2018). Among the  $\text{PM}_{2.5}$  concentration distributions, Politecnico and Lingotto and Consolata and Rubino trends are similar ( $7 \mu\text{g}/\text{m}^3$  for Politecnico and Lingotto and  $8 \mu\text{g}/\text{m}^3$  for Consolata and Rubino). Based on the 3 years of observations, the probability of exceeding the daily limit ( $25 \mu\text{g}/\text{m}^3$ ) for these stations was 21.6%. The distribution mode in Rebaudengo and Grassi stations ( $10 \mu\text{g}/\text{m}^3$ ) was more centered than in the other conditions. For these stations, the probability of exceeding the legal limit was 27.1%. The  $\text{PM}_{10}$  concentrations showed three different distributions for all six stations. In Politecnico and Lingotto stations, the mode occurred at  $12 \mu\text{g}/\text{m}^3$ . For Consolata and Rubino stations, the mode was  $17 \mu\text{g}/\text{m}^3$ ; for Rebaudengo and Grassi stations, it was  $20 \mu\text{g}/\text{m}^3$ . The probabilities of exceeding the threshold value for Politecnico and Lingotto, Consolata and Rubino, and Rebaudengo and Grassi stations were 14.31%, 17.59%, and

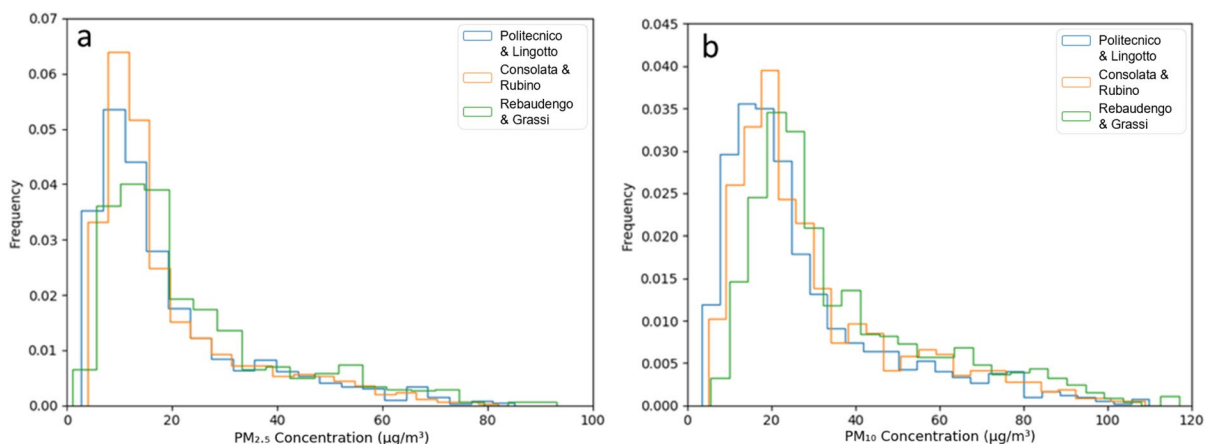


**Fig. 4** a  $\text{PM}_{2.5}$  and b  $\text{PM}_{10}$  concentration distribution at the six stations Politecnico and Lingotto in blue, Consolata and Rubino in orange, and Rebaudengo and Grassi in green

23.14%, respectively. Unlike the case of  $PM_{2.5}$ , for  $PM_{10}$ , there was a noticeable difference between the different conditions. This difference could be attributable to the more significant influence of local conditions on  $PM_{10}$  than  $PM_{2.5}$ , as the authors evidenced in (Boanini et al., 2021).

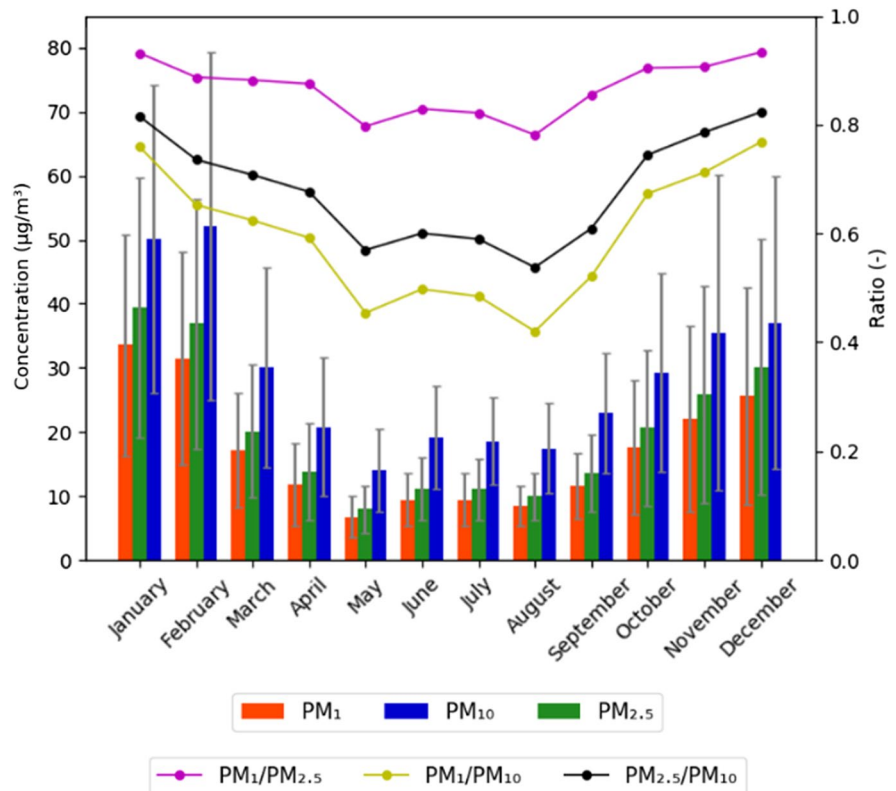
Temporal variation

Monthly variation of pollutants

Figure 5 shows the monthly variations of  $PM_1$ ,  $PM_{2.5}$ , and  $PM_{10}$  concentrations and the monthly ratios of  $PM_1/PM_{10}$ ,  $PM_{2.5}/PM_{10}$ , and  $PM_1/PM_{2.5}$ . The data were derived from the mean of the background station at Turin Polytechnic in the period between September 2018 and September 2021. The overall means over the 3 years for  $PM_1$ ,  $PM_{2.5}$ , and  $PM_{10}$  were  $20 \mu\text{g}/\text{m}^3$ ,  $20 \mu\text{g}/\text{m}^3$ , and  $29 \mu\text{g}/\text{m}^3$ , respectively. In all 3 years, the maximum limit of daily  $PM_{10}$  exceedance (35 days/year for  $PM_{10} > 50 \mu\text{g}/\text{m}^3$ ) was surpassed. The mean  $PM_1/PM_{2.5}$  ratio was 0.85, and the  $PM_{2.5}/PM_{10}$  ratio was 0.69.

The figure reveals a noticeable V-shaped variation in concentrations and ratios over the months. This trend is similar for all three particulate fractions. The highest concentrations were recorded in the winter months, at the beginning and end of each year. The peaks occurred in January and February, which are generally characterized by haze pollution due to atmospheric conditions favorable to accumulation in the lower layer of the atmosphere (Maurizi et al., 2013). Furthermore, in these months, the  $PM_{2.5}/PM_{10}$  ratio is generally higher, reflecting the difference in sources between summer and winter conditions (Choi et al., 2013). Several studies have evaluated the impacts of typical winter heating sources, such as domestic boilers, in the area under study (Pognant et al., 2017) and the entire Po Valley (Gilardoni et al., 2020). The concentration was lowest in the summer months, especially in May. The spring months showed a gradual reduction in concentrations, whereas the autumn months showed an increase. The same trend was also found by (Chen et al., 2016; Xu et al., 2017). The monthly variations of the  $PM_1/PM_{10}$  and  $PM_{2.5}/PM_{10}$  ratios were more sensitive than the

**Fig. 5** Monthly variations of  $PM_1$ ,  $PM_{2.5}$ , and  $PM_{10}$  concentrations and their ratios at the Polytechnic station between September 2018 and September 2021. The gray bar represents the oscillation range



variation of the  $PM_1/PM_{2.5}$  ratio. The latter had an almost constant trend throughout the months, with only a slight reduction in the summer. The first two ratios showed a summer month reduction with respect to the annual mean of 17.11% and 15.62%, respectively. However, the  $PM_1/PM_{2.5}$  ratio had a reduction of 4.76%. To determine the statistical significance of the observed seasonal variation, a Kruskal–Wallis  $H$  test was performed among the seasons. The test confirmed significant differences for  $PM_1/PM_{10}$  ( $H=206.41$ ,  $p<0.000$ ),  $PM_{2.5}/PM_{10}$  ( $H=194.65$ ,  $p<0.000$ ), and  $PM_1/PM_{2.5}$  ( $H=225.75$ ,  $p<0.000$ ). Further, Dunn's tests identified a significant reduction in  $PM_1/PM_{10}$  ( $p<0.000$ ) and  $PM_{2.5}/PM_{10}$  ( $p<0.001$ ) during the summer months compared to the winter. The observed differences in winter and summer particulates can be explained by the different sources, and atmospheric conditions have a greater impact on the coarse fraction than the fine fraction

(Pecorari et al., 2013; Pernigotti et al., 2012). To provide additional details, the correlations of  $PM_1$  with  $PM_{2.5}$  and  $PM_{10}$  were studied on the basis of different seasons.

In all seasons, the correlation between  $PM_1$  and  $PM_{2.5}$  was greater than 0.95 ( $p<0.01$ ), as shown in Fig. 6. Moreover, the regression line had a similar slope in winter, autumn, and spring. However, in summer, the regression line had a lower slope. The  $PM_1/PM_{10}$  coefficient of determination varied from a maximum of 0.91 in winter to a minimum of 0.88 in summer. Similarly, the  $PM_{2.5}/PM_{10}$  ratio reached its maximum value during winter. Autumn and spring showed a similar slope, but summer had the minimum value (0.41,  $p<0.01$ ). The latter was attributable to the greater involvement of fine particles in photochemical reactions (Carbone et al., 2010; Wang et al., 2016). In autumn and winter, some points deviated from the global trend, showing higher

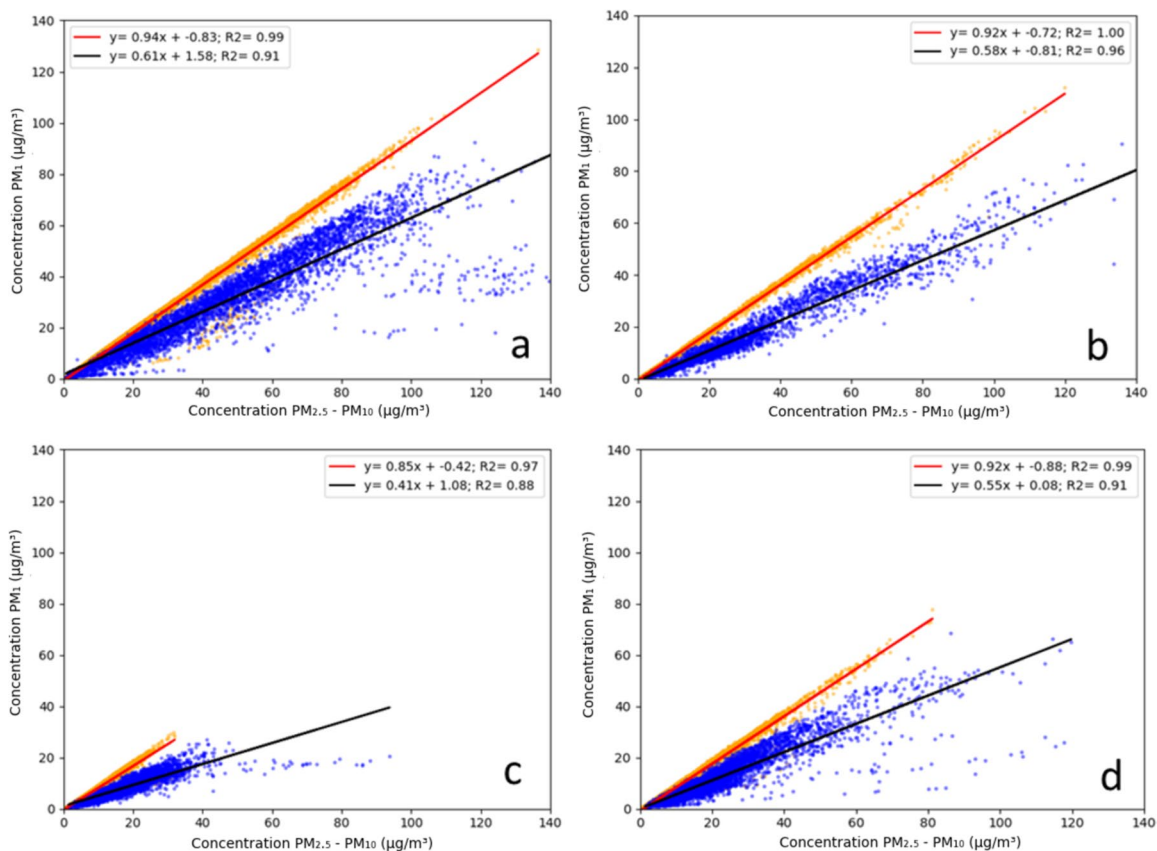


**Fig. 6** Correlations between  $PM_1$  concentration and  $PM_{2.5}$  concentration (orange) and between  $PM_1$  concentration and  $PM_{10}$  concentration (blue) on a seasonal basis **a** winter, **b** spring, **c** summer, and **d** autumn.  $R^2 = R$ -squared

concentrations of  $PM_{10}$  in correspondence with low values of  $PM_1$ . This is a typical behavior of a large pollution circumstance, as also noted by X. Li et al., (2017a, b) and Xue et al. (2020). Our results align with Davtalab et al. (2023), who found higher  $PM_{2.5}$  and  $PM_{10}$  concentrations in winter, peaking in January and February, and the lowest in summer. They attributed April  $PM_{10}$  peaks to road dust from winter tires. They also noted the highest  $PM_{2.5}/PM_{10}$  ratios in winter and lowest in summer, consistent with our findings, indicating a higher proportion of fine particles in winter due to increased combustion and stable atmospheric conditions (Davtalab et al., 2023). Further, Bamola et al. (2024) found that the lowest concentrations of both  $PM_{2.5}$  and  $PM_{10}$  occurred during the monsoon season (July and August) due to precipitation and higher wind speeds aiding pollutant dispersion. The highest concentrations were recorded in November and December, similar to our findings, attributed to increased biomass burning.

### Hourly and seasonal variations of pollutants

Several natural and anthropic factors affect the concentration levels of particulate matter during the day. The most important are direct emissions, secondary particulate formation, dilution or removal processes, and variation of the height of the PBL (Maurizi et al., 2013; Pecorari et al., 2013; Sullivan et al., 2016). Based on the 3 years of observations, the hourly data through the day were processed to obtain evidence of these processes affecting

concentration. In addition, the season-based variation was studied to highlight the hourly evolution of  $PM$  concentration.

For the particulate fractions shown in Fig. 7, there was significant hourly variation throughout the day. The variation was more pronounced for  $PM_{10}$  than for  $PM_{2.5}$  or  $PM_1$ . In particular, the values of  $PM_{2.5}$  and  $PM_1$  were substantially stable at night, and their morning increase was reduced compared to that of  $PM_{10}$ . The nocturnal decrease of  $PM_{10}$  is attributable to dry deposition, as suggested by Li et al. (2019), whereas the concentration increase from 7:00 to 9:00 AM is typical of the traffic schedule (Chen et al., 2020). For all fractions, after the peak, there was a decline in the afternoon due to the height of the planetary limit state (Du et al., 2013; Su et al., 2018). The dilution peak occurred at 5:00 PM. Subsequently, the evening increase in transport and nighttime stability caused concentrations to increase (Chen et al., 2016). The contribution of heating sources influences particulate concentrations with increases during the evening and night periods. These results align with other studies that conducted a comprehensive analysis of the daily cycle of pollutants in urban areas. Elansky et al. (2020) observed that night concentrations of  $PM_{10}$  decrease and reach their minima early in the morning (around 4:00–4:30 AM), followed by a rapid increase starting from 5:00 AM due to morning rush hour traffic. The peak concentrations were observed around 8:00–9:00 AM. This morning peak is attributed to the combination of heavy traffic and the breakdown of surface temperature inversions, which

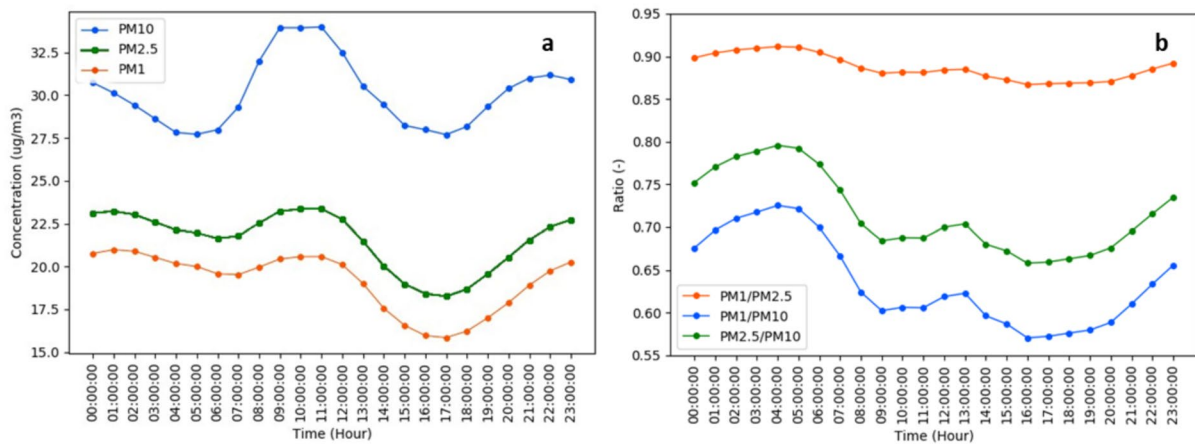


**Fig. 7** Hourly mean variations of  $PM_1$ ,  $PM_{2.5}$ , and  $PM_{10}$  **a** concentrations and **b** ratios

typically occurs around 7:00 AM in summer and 9:00 AM in winter.

The  $PM_1/PM_{10}$  and  $PM_{2.5}/PM_{10}$  ratios shown in Fig. 7 had a fairly similar shape throughout the day. As confirmation, the  $PM_1/PM_{2.5}$  ratio had a very narrow fluctuation throughout the day, with an amplitude of 0.05, while the  $PM_1/PM_{10}$  and  $PM_{2.5}/PM_{10}$  ratios had amplitudes of 0.16 and 0.13, respectively. In comparison to the hourly concentration trend curves, the ratio trends are out of phase. More precisely, the absolute peaks for  $PM_1/PM_{10}$  and  $PM_{10}/PM_{10}$  were reached at 4:00 AM during the relative minimums of  $PM_{10}$  concentration. This confirms a greater nocturnal removal of coarse fractions than fine particles (Galindo et al., 2018). Finally, the ratio decreased from 7:00 AM to 9:00 AM and reached a maximum at about 1:00 PM. The maximum seemed to be attributable to the higher dilution rate of coarse particles than fine particles, as proven by (Lestari et al., 2003). Furthermore, this peak occurred at the time of maximum solar radiation, which affects the secondary formation processes of particulate matter. Typically, secondary training involves fine fractions to a greater extent (Squizzato et al., 2017; Sullivan et al., 2016; Wang et al., 2016).

To perceive the daily concentration variation more thoroughly, Fig. 8 illustrates the differences in trends during the four seasons, and Fig. 9 shows the differences between workdays and weekend days.

According to Fig. 8, and confirming previous analysis, the highest concentrations occurred in winter, the lowest occurred in summer, and autumn values were higher than spring values.

During the day, the intensity fluctuations varied according to season. Winter had the greatest fluctuation, and summer had the least. The daily percentage variations of  $PM_1$ ,  $PM_{2.5}$ , and  $PM_{10}$  were 33.1%, 30.44%, and 24.8% in winter and 25.4%, 20.4%, and 20.9% in summer. This indicates that the height of the PBL, which is lower in winter than in summer, strongly affects the daily concentration fluctuation (Maurizi et al., 2013). As subsidence tends to increase concentrations, radiance produces daily variation in the accumulation and dilution of contaminants (Chen et al., 2016). The fluctuations in spring and autumn were minor in comparison to those in winter but greater than those in summer. The daily oscillations in  $PM_1$ ,  $PM_{2.5}$ , and  $PM_{10}$  were 26.8%, 23.9%, and 21.7% in spring and 29.5%, 27.4%, and 23.9%

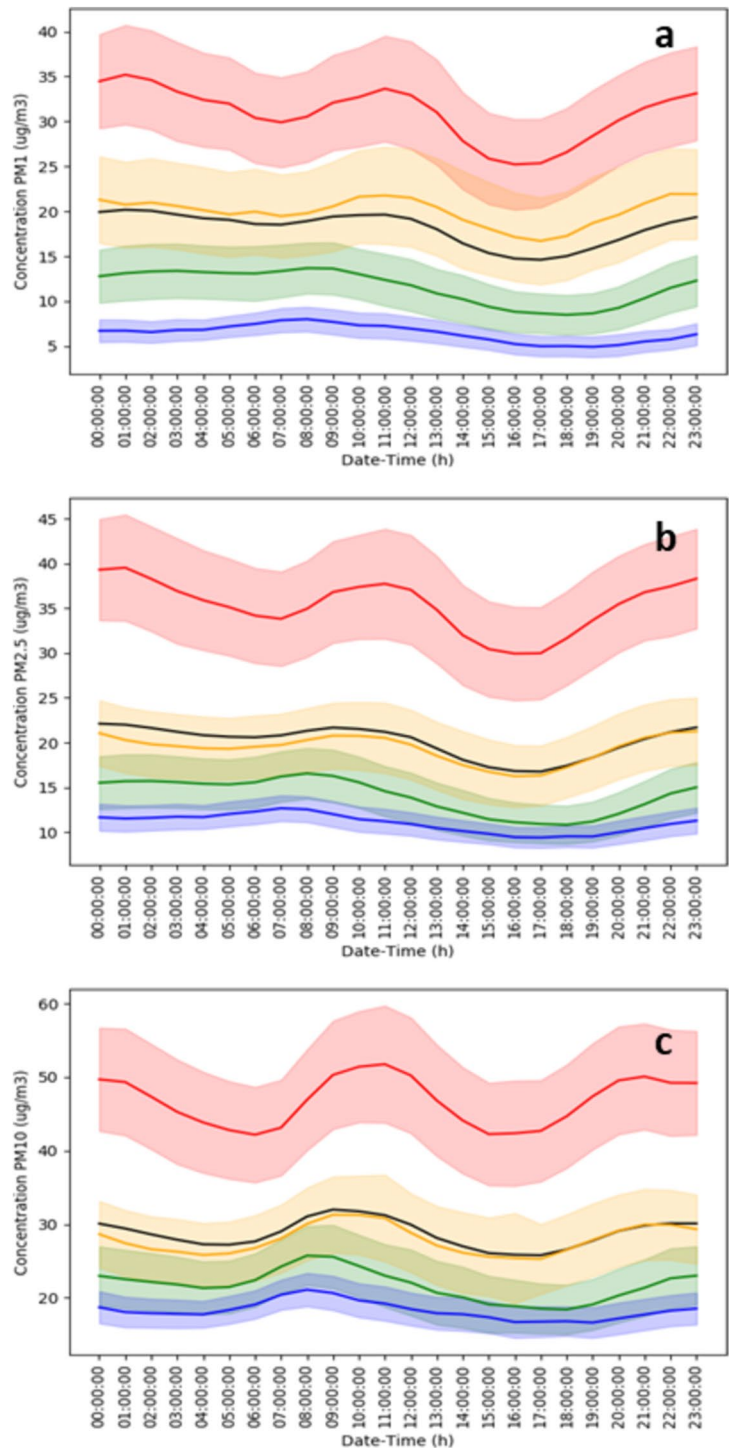
in autumn, respectively. Autumn and winter had similar inter-day variation behaviors, as did spring and summer, confirming the observations of Chen et al. (2016), R. Li et al., (2017a, b), and Zhao et al. (2018). One of the most important aspects of these trends is the diurnal concentration peak. In winter and autumn, the peak occurred at 11:00 AM. In summer and spring, it occurs at 9:00 AM. This contrasts with studies in different contexts. For example, Bamola et al. (2024) observed that  $PM_{2.5}$  and  $PM_{10}$  concentrations were higher during the morning (around 9:00 AM) and lower in the early evening (4:00–5:00 PM) without seasonal changes.

#### Differences between weekend and workday trends

An important aspect of the analysis of temporal variation, the differences between weekend days (Saturday, Sunday, and holidays) and workdays (all other days) are illustrated in Fig. 9. The mean daily concentrations of  $PM_1$  ( $z=42,281$ ;  $p>0.1$ ) and  $PM_{2.5}$  ( $z=42,695$ ;  $p>0.1$ ) were not significantly different in weekend days and workdays.  $PM_1$  had a very low difference in concentration ( $<1 \mu\text{g}/\text{m}^3$ ) between weekend days and workdays (both about  $19 \mu\text{g}/\text{m}^3$ ). Also for  $PM_{2.5}$ , the difference between workdays ( $22 \mu\text{g}/\text{m}^3$ ) and weekend days ( $21 \mu\text{g}/\text{m}^3$ ) was very low about  $1 \mu\text{g}/\text{m}^3$ . On the other hand, for  $PM_{10}$ , there was a reduction ( $z=17,142$ ;  $p<0.05$ ) on weekend days ( $29 \mu\text{g}/\text{m}^3$ ) compared to workdays ( $31 \mu\text{g}/\text{m}^3$ ). The difference between the two classes of days was  $2 \mu\text{g}/\text{m}^3$ .

For all fractions, the hourly trends through a day showed a greater amplitude on workdays than on weekend days. The morning hour increase and afternoon decrease are more marked for workdays (orange curve). Unlike the results of Chen et al. (2016), the concentration peak was about 2 h ahead on weekends. Furthermore, for  $PM_{2.5}$  and  $PM_1$ , the relative and absolute minimum values were advanced by 1 h. Conversely, Zhang et al. (2021) conducted a similar analysis in Shanghai and found a noticeable weekend effect on  $PM_{10}$  concentrations, with higher values observed on weekdays compared to weekends. While aligning with our findings on  $PM_{10}$ , they observed also CO and NO<sub>x</sub> to trace differences in vehicular emissions and human activities between weekdays and weekends.

**Fig. 8** Hourly mean variations of **a** PM<sub>1</sub>, **b** PM<sub>2.5</sub>, and **c** PM<sub>10</sub>. Different colours represent the four seasons winter (red), autumn (yellow), spring (green), and summer (blue). The shaded area represents the 95% confidence interval. The black line represents the overall annual mean concentration



The mean PM<sub>1</sub>/PM<sub>10</sub> ratio was 0.67 on weekend days and 0.62 on workdays. The mean PM<sub>2.5</sub>/PM<sub>10</sub> ratio was 0.75 on weekend days and 0.70 on workdays. Hence, PM<sub>1</sub>/PM<sub>2.5</sub> was 0.89 and 0.86 on

weekend days and workdays, respectively. In each ratio, the weekend days had a higher value than the workdays. Generally, there is a prevalence of fine particles at night on workdays. In the other hours,

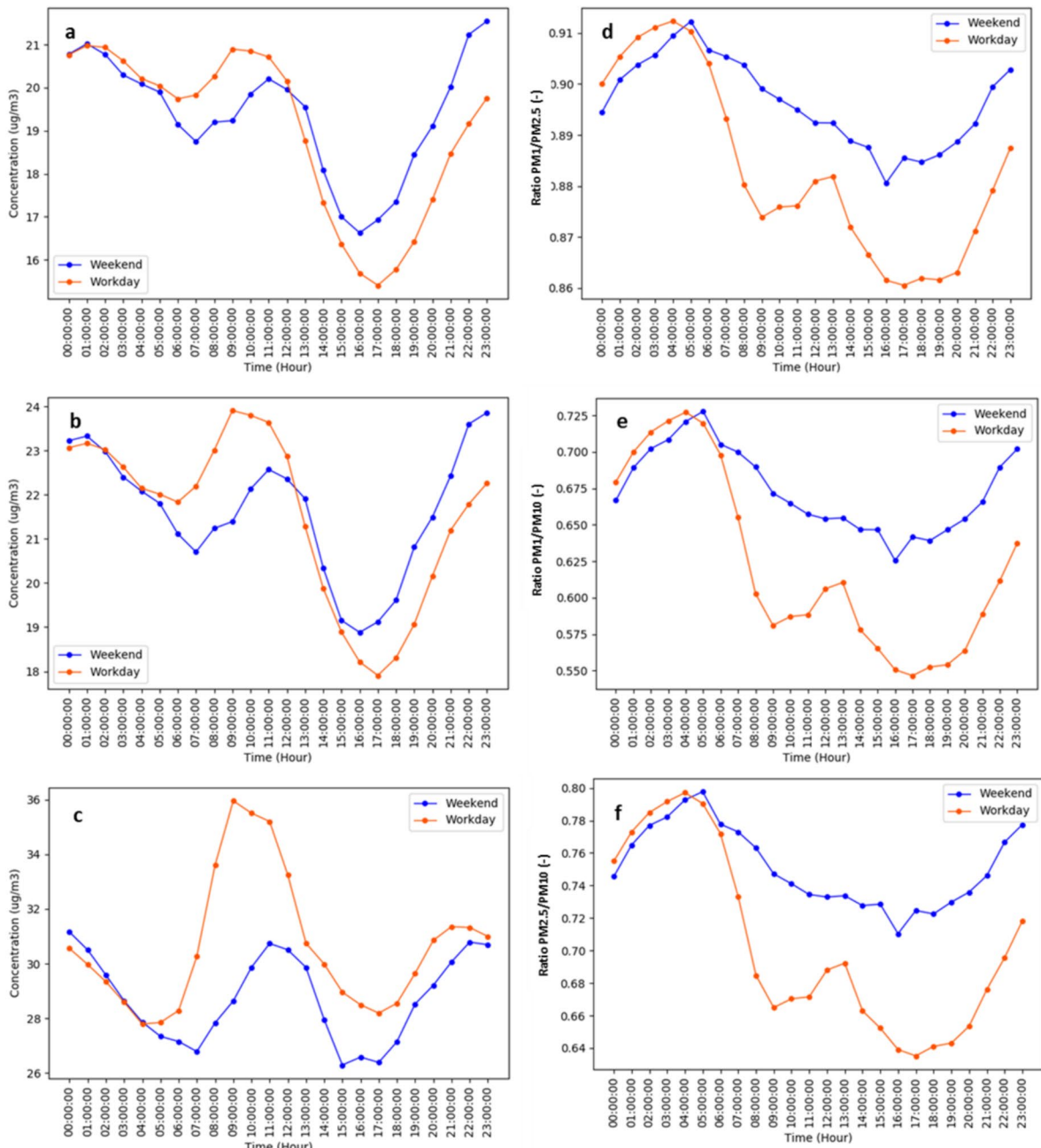


**Fig. 9** Top, hourly trends in weekend day (blue) and workday (orange) **a**  $PM_1$ , **b**  $PM_{2.5}$ , and **c**  $PM_{10}$  concentrations. Bottom, hourly trends in the weekend day and workday **d**  $PM_1/PM_{2.5}$ , **e**  $PM_1/PM_{10}$ , and **f**  $PM_{2.5}/PM_{10}$  ratios

the weekend day curve is higher. This means that the weekend days are affected by a higher proportion of fine particles in comparison to  $PM_{10}$  than the workdays. An interesting element of this evaluation is the different trends for the two cases, which were

verified by all three ratios considered. From 9:00 AM to 1:00 PM, there was an increase in workday ratios. This did not occur on weekend days, for which the line is U-shaped with a minimum in the afternoon.

The differences in the trends can be attributed to the different traffic flows on weekend days and workdays (Giugliano et al., 2005; Lonati et al., 2011). Traffic is the only source that is reduced during the weekend (Chang et al., 2015). As was observed recently by Filigrana et al. (2020) in a traffic study in the Po Valley, and also in the present case, the weekend-day traffic reduction provides reductions in concentrations and substantial changes in the relationships between fine and coarse fractions. Additionally, Zhang et al. (2021) observed that the weekend effect varied seasonally, with a stronger effect in spring and autumn. This seasonal dependence was linked to changes in photochemical activity and meteorological conditions as well, which is consistent with our findings that highlight the influence of atmospheric conditions on particulate concentrations throughout the year.

Figure 10 shows the percentage differences from the weekly mean value for each day of the week for each of the four seasons. Considering the differences between weekend day and workday concentrations, the objective was to verify how the concentrations were distributed throughout the week and which days were more polluted than the seasonal mean pollution.

PM<sub>10</sub> concentrations had a similar pattern to PM<sub>1</sub> and PM<sub>2.5</sub> fractions in summer and spring. However, the PM<sub>10</sub> concentrations in autumn and winter formed a different trend. In summer, Thursday had the highest mean values: +10.64% for PM<sub>10</sub>, +11.91% for PM<sub>2.5</sub>, and +13.69% for PM<sub>1</sub>. Saturday and Sunday had values below the mean, but the Sunday reductions were about 10% for PM<sub>1</sub> and PM<sub>2.5</sub> and 14.35% for PM<sub>10</sub>. Mondays showed a substantial reduction of PM<sub>1</sub> and PM<sub>2.5</sub>, but the coarse fraction concentration was consistent with the global mean. In spring,

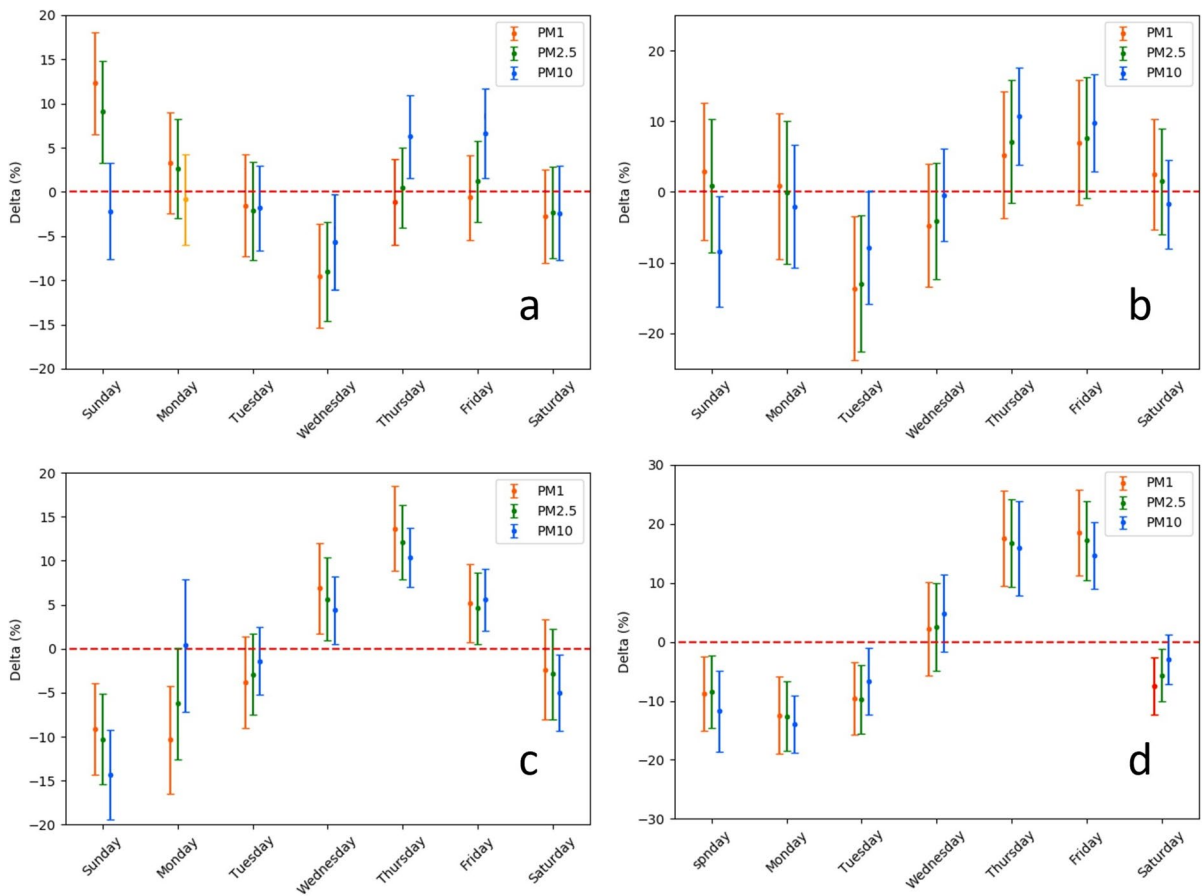


**Fig. 10** Day-of-week trends of PM<sub>1</sub>, PM<sub>2.5</sub>, and PM<sub>10</sub> in the different seasons **a** winter, **b** autumn, **c** summer, and **d** spring. Error bars represent the 95% confidence interval. The red dot line represents the weekly mean value

Thursdays and Fridays had increases compared to the mean of more than 15%. On the other hand, in addition to weekend days, Mondays and Tuesdays had concentrations 10% lower than the mean. In winter, the concentration peaks of  $PM_{10}$  and  $PM_{2.5}$  occurred on Sunday (+12.3% and 9.6%), followed by a linear reduction until Wednesday, when changes of  $-8.8\%$  and  $-9.5\%$  were recorded. The  $PM_{10}$  fraction had fewer variations during the week, with two days at higher concentration. Similarly, in autumn, the minimum occurred on Tuesday, and Thursday and Friday had the highest values.

Globally, summer and spring had lower values on weekends and higher values on workdays. In autumn and winter, the minimum was in the middle of the week, and the highest values occurred on the weekend. As in Fig. 8, similar trends were observed in autumn and winter and in spring and summer. The findings of Peccarrisi et al. (2024) corroborate our results. They observed that  $PM_{2.5}$  and  $PM_{10}$  concentrations exhibited higher values from Tuesday to Friday and decreased over the weekend due to reduced human activities. Peccarrisi et al. (2024) also highlighted that the weekly cycle of  $PM_{2.5}$  concentrations showed seasonal variations. In winter and spring, all sites presented larger values on Friday, with a significant increase from Tuesday to Friday, followed by a decrease during weekends. Additionally, some analogies can be drawn from our evidence and the findings of Xue et al. (2020), who investigated the day-of-week patterns of  $PM_{0.1}$ , components such as organic carbon and elemental carbon. They found a similar trend in organic carbon, suggesting an increased

impact of biomass combustion during the winter and autumn seasons. They found a similar trend in organic carbon, suggesting an increased impact of biomass combustion during the winter and autumn seasons. This observation is further supported by the evidence from Pognant et al. (2017), who studied annual and seasonal concentrations of ultrafine particulate matter in a geographic context similar to ours. Their research highlighted the emissions of biomass boilers under different scenarios.

#### Source direction

The results of CPF are shown in Fig. 11. As shown, similar configurations were obtained for all three particulate classes. There is a low probability of concentrations greater than the 75th percentile in the N–NE–E angular sectors. High probabilities occur in the opposite S–SW–W angular sectors. This result has particular interest as these are typical directions for long-range particle transport involving Saharan dust. For high concentration values, there are no significant influences in the direction of the Po Valley (NE–E). This confirms that the phenomenon of major pollution due to subsidence is homogeneous and involves the entire Po Valley (Arvani et al., 2016; Diémoz et al., 2019).

The graphs in Fig. 12 show the combinations of wind speed and direction at the measurement site. The color intensity indicates the concentration recurrence probability for each selected concentration range. As shown, there were different results for the three analyzed particulate fractions. The finer

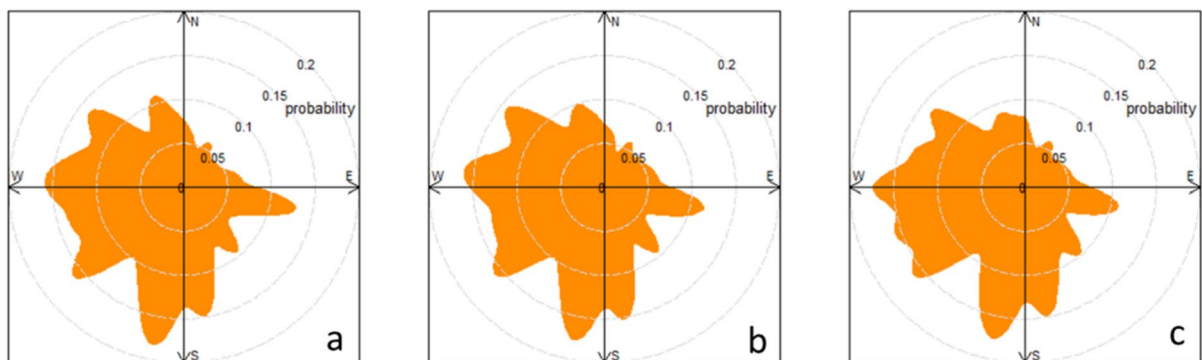


**Fig. 11** Conditional probability function (CPF) plots for the Polytechnic station for **a**  $PM_{10}$ , **b**  $PM_{2.5}$ , and **c**  $PM_{10}$  concentrations > 75th percentile

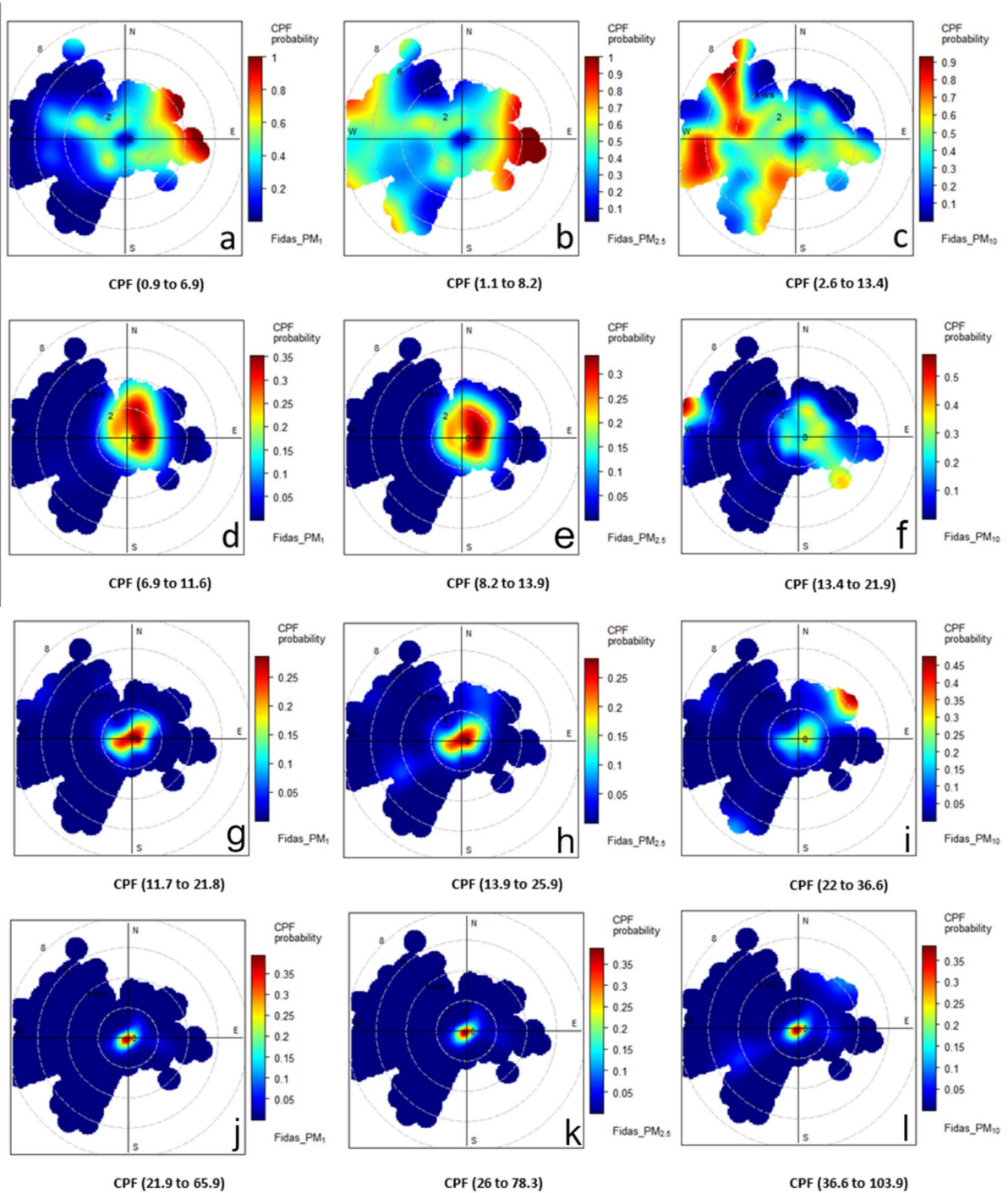


**Fig. 12** Conditional bivariate probability function plots for four intervals of PM<sub>1</sub>, PM<sub>2.5</sub>, and PM<sub>10</sub> hourly concentrations at the Polytechnic station. CBPF probability is indicated by the color scale. The interval shown below the graphs corre-

sponds to the four quartiles of the PM values 1–25%, 25–50%, 50–75%, and 75–99%. Each circle represents the wind intensity (from 2 to 8 m/s), and the perpendicular axis represents the compass (wind direction N, S, W, E)

fractions ( $PM_1$  and  $PM_{2.5}$ ) showed a prevalence of low concentrations (first quartile) when the wind blows from the east with an intensity range from 4 to 6. This phenomenon could be attributed to the aerosol contribution of the PM concentrations in the Po Valley which is in an easterly direction with respect to the measurement point according to Diémoz et al. (2019). On the other hand, the  $PM_{10}$  prevalent in the first quartile occurred when the wind was from the NW–W with varying speeds (2–8 m/s). For the second quartile, the highest probabilities were gathered around the origin, at low speeds (<4 m/s) and with a slight prevalence of NE direction.

For the last two quartiles, the highest probabilities for all the PM fractions are concentrated on the origin. Instead, there was a slight probability for the NE–SW line for  $PM_{2.5}$  and  $PM_{10}$ . These directions represent the two major openings of the city of Turin toward the Po Valley. In fact, in the E–SE direction, the city is separated by a hill; on the opposite side, it is surrounded by the Alps. The S–SW direction is therefore the main arrival direction of particulates during Saharan events (fourth quartile) (Diémoz et al., 2021; Tositti et al., 2014). This also confirms the result illustrated in Fig. 11 regarding the preponderance of concentrations in the fourth quartile in the S–SW direction.

## Conclusion

The present study analyzed the spatial and temporal variations of  $PM_1$ ,  $PM_{2.5}$ , and  $PM_{10}$  concentrations in the metropolitan city of Turin from 2018 to 2021. The study also provided an analysis of the direction of sources through a conditional probability analysis. Although the study focused on a specific area of the Po Valley, it is representative of different conditions of diffusion of contaminants in urban environments that were investigated.

In this environmental context, as the urban context changed were substantial differences in  $PM_{10}$  concentration. In particular, the lowest concentrations were recorded in the background environment ( $29 \mu\text{g}/\text{m}^3$ ), and the maximum occurred at traffic stations ( $36 \mu\text{g}/\text{m}^3$ ).  $PM_{2.5}$  concentrations in the background environment were about  $20 \mu\text{g}/\text{m}^3$ . However, at the traffic stations, concentrations were significantly higher ( $24 \mu\text{g}/\text{m}^3$ ). Large fluctuations in concentrations were

observed across the seasons and throughout the day. Due to the predisposing atmospheric conditions and a greater contribution of sources (such as domestic heating and biomass burning), the winter months had higher concentration values of the three observed PM fractions ( $PM_1$ ,  $PM_{2.5}$ , and  $PM_{10}$ ). Furthermore, the central hours of the day and the evening were affected by higher concentrations. Daily variation in concentrations was more pronounced in the winter and autumn than in the summer and spring. The traffic effect on particulate concentration was assessed by observing the differences in concentration between weekend days and workdays.  $PM_1$ ,  $PM_{2.5}$ , and  $PM_{10}$  values were 1.81%, 1.84%, and 6.14% lower on weekend days than on workdays. Furthermore, the hourly trends through the day differed in times of relative maximum and minimum concentrations. Finally, applying CPF and CBPF to pollutant concentrations and wind speed and direction highlighted the ways in which the local pollution of the city of Turin is conditioned by global phenomena. The major external particulate contributions, observed in the first and second quartiles (Fig. 12), were from the N–NE, direction of Po Valley. However, for all PM fractions, there was a contribution from the S–SW, the typical direction of Saharan dust transport.

The results of the present study could help decision-makers adopt restrictive policies and measures to reduce pollution in specific areas or specific time periods. Furthermore, the study provides researchers with a general framework of particulate concentrations in different contexts. Similar findings have been reported globally, highlighting the need for tailored air quality management plans that consider specific urban contexts (Karagulian et al., 2015). Additional studies will be needed to evaluate the influences of meteorological phenomena that contribute to the dilution of contaminants (such as rain and wind) to the spatial and temporal variations of particulate concentrations. For instance, in-depth investigations on seasonal variations and the role of meteorological conditions can provide further insights into effective pollution control measures (Briggs & Long, 2016). Finally, in a geographically adverse context such as the Po Valley, an assessment of how emission reduction policies (e.g., traffic blocks) would affect the spatial and temporal variations of contaminants could be a useful further line of research. This is in line with other studies calling for studying how targeted

policies, including traffic restrictions and improved public transportation, can lead to significant reductions in particulate matter concentrations and improve overall air quality (Vyas & Varia, 2023).

**Author contribution** Domenico Mecca: Conceptualization, Formal Analysis, Methodology, Writing—Original Draft Chiara Boanini: Conceptualization, Software, Validation, Writing—Review & Editing Vincenzo Vaccaro: Resources, Data curation, Writing—Review & Editing, Visualization Davide Gallione and Nicole Mastromatteo: Resources Marina Clerico: Resources, Supervision, Project administration, Funding acquisition. All authors reviewed the manuscript.

**Data availability** No datasets were generated or analysed during the current study.

**Declarations**

**Competing interests** The authors declare no competing interests.

**Open Access** This article is licensed under a Creative Commons Attribution-NonCommercial-NoDerivatives 4.0 International License, which permits any non-commercial use, sharing, distribution and reproduction in any medium or format, as long as you give appropriate credit to the original author(s) and the source, provide a link to the Creative Commons licence, and indicate if you modified the licensed material. You do not have permission under this licence to share adapted material derived from this article or parts of it. The images or other third party material in this article are included in the article's Creative Commons licence, unless indicated otherwise in a credit line to the material. If material is not included in the article's Creative Commons licence and your intended use is not permitted by statutory regulation or exceeds the permitted use, you will need to obtain permission directly from the copyright holder. To view a copy of this licence, visit <http://creativecommons.org/licenses/by-nc-nd/4.0/>.

**References**

Arvani, B., Pierce, R. B., Lyapustin, A. I., Wang, Y., Ghermandi, G., & Teggi, S. (2016). Seasonal monitoring and estimation of regional aerosol distribution over Po valley, northern Italy, using a high-resolution MAIAC product. *Atmospheric Environment*, *141*, 106–121. <https://doi.org/10.1016/j.atmosenv.2016.06.037>

Ashbaugh, L. L., Malm, W. C., & Sadeh, W. Z. (1985). A residence time probability analysis of sulfur concentrations at grand Canyon National Park. *Atmospheric Environment*, *19*(19), 1263–1270. [https://doi.org/10.1016/0004-6981\(85\)90256-2](https://doi.org/10.1016/0004-6981(85)90256-2)

Atamaleki, A., Motesaddi Zarandi, S., Fakhri, Y., Abouee Mehrizi, E., Hesam, G., Faramarzi, M., & Darbandi, M.

(2019). Estimation of air pollutants emission (PM10, CO, SO2 and NOx) during development of the industry using AUSTAL 2000 model: A new method for sustainable development. *MethodsX*, *6*, 1581–1590. <https://doi.org/10.1016/j.mex.2019.06.010>

Atkinson, R. W., Butland, B. K., Dimitroulopoulou, C., Heal, M. R., Stedman, J. R., Carslaw, N., Jarvis, D., Heavyside, C., Vardoulakis, S., Walton, H., & Anderson, H. R. (2016). Long-term exposure to ambient ozone and mortality: A quantitative systematic review and meta-analysis of evidence from cohort studies. *British Medical Journal Open*, *6*, 1–10. <https://doi.org/10.1136/bmjopen-2015-009493>

Bastola, U., & Sapkota, P. (2015). Relationships among energy consumption, pollution emission, and economic growth in Nepal. *Energy*, *80*, 254–262. <https://doi.org/10.1016/J.ENERGY.2014.11.068>

Batterman, S., Ganguly, R., & Harbin, P. (2015). High resolution spatial and temporal mapping of traffic-related air pollutants. *IJERPH*, *12*, 3646–3666. <https://doi.org/10.3390/ijerph120403646>

Bo, M., Charvolin-Volta, P., Clerico, M., Nguyen, C. V., Pognant, F., Soulhac, L., & Salizzoni, P. (2020). Urban air quality and meteorology on opposite sides of the Alps: The Lyon and Torino case studies. *Urban Climate*, *34*, 100698. <https://doi.org/10.1016/j.uclim.2020.100698>

Boanini, C., Mecca, D., Pognant, F., Bo, M., & Clerico, M. (2021). Integrated mobile laboratory for air pollution assessment: Literature review and cc-TrAIRer design. *Atmosphere*, *12*(8), 1004. <https://doi.org/10.3390/atmos12081004>

Bozzola, M., & Swanson, T. (2014). Policy implications of climate variability on agriculture: Water management in the Po river basin, Italy. *Environmental Science & Policy*, *43*, 26–38. <https://doi.org/10.1016/J.ENVSCI.2013.12.002>

Brook, R. D., Newby, D. E., & Rajagopalan, S. (2017). The global threat of outdoor ambient air pollution to cardiovascular health. *JAMA Cardiology*, *2*, 353. <https://doi.org/10.1001/jamacardio.2017.0032>

Campanelli, M., Iannarelli, A. M., Mevi, G., Casadio, S., Diémoz, H., Finardi, S., Dinoi, A., Castelli, E., Di Sarra, A., Di Bernardino, A., Casasanta, G., Bassani, C., Siani, A. M., Cacciani, M., Barnaba, F., Di Liberto, L., & Argentini, S. (2021). A wide-ranging investigation of the COVID-19 lockdown effects on the atmospheric composition in various Italian urban sites (AER – LOCUS). *Urban Climate*, *39*, 100954. <https://doi.org/10.1016/j.uclim.2021.100954>

Carbone, C., Decesari, S., Mircea, M., Giulianelli, L., Finessi, E., Rinaldi, M., Fuzzi, S., Marinoni, A., Duchi, R., Perrino, C., Sargolini, T., Varde, M., Sprovieri, F., Gobbi, G. P., Angelini, F., & Facchini, M. C. (2010). Size-resolved aerosol chemical composition over the Italian Peninsula during typical summer and winter conditions. *Atmospheric Environment*, *44*, 5269–5278. <https://doi.org/10.1016/J.ATMOSENV.2010.08.008>

Caserini, S., Giani, P., Cacciamani, C., Ozgen, S., & Lonati, G. (2017). Influence of climate change on the frequency of daytime temperature inversions and stagnation events in the Po Valley: Historical trend and future projections. *Atmospheric Research*, *184*, 15–23. <https://doi.org/10.1016/J.ATMOSRES.2016.09.018>

- Chang, S. Y., Vizuete, W., Valencia, A., Naess, B., Isakov, V., Palma, T., Breen, M., & Arunachalam, S. (2015). A modeling framework for characterizing near-road air pollutant concentration at community scales. *Science of the Total Environment*, 538, 905–921. <https://doi.org/10.1016/j.scitotenv.2015.06.139>
- Chen, T., He, J., Lu, X., She, J., & Guan, Z. (2016). Spatial and temporal variations of PM<sub>2.5</sub> and its relation to meteorological factors in the urban area of Nanjing, China. *International Journal of Environmental Research and Public Health*, 13, 921. <https://doi.org/10.3390/ijerph13090921>
- Chen, G., Li, S., Zhang, Y., Zhang, W., Li, D., Wei, X., He, Y., Bell, M. L., Williams, G., Marks, G. B., Jalaludin, B., Abramson, M. J., & Guo, Y. (2017). Effects of ambient PM<sub>1</sub> air pollution on daily emergency hospital visits in China: An epidemiological study. *The Lancet Planetary Health*, 1, e221–e229. [https://doi.org/10.1016/S2542-5196\(17\)30100-6](https://doi.org/10.1016/S2542-5196(17)30100-6)
- Chen, M., Guo, S., Hu, M., & Zhang, X. (2020). The spatiotemporal evolution of population exposure to PM<sub>2.5</sub> within the Beijing-Tianjin-Hebei urban agglomeration, China. *Journal of Cleaner Production*, 265, 121708. <https://doi.org/10.1016/j.jclepro.2020.121708>
- Choi, J., Heo, J.-B., Ban, S.-J., Yi, S.-M., & Zoh, K.-D. (2013). Source apportionment of PM<sub>2.5</sub> at the coastal area in Korea. *Science of the Total Environment*, 447, 370–380. <https://doi.org/10.1016/j.scitotenv.2012.12.047>
- Conte, M., Dinoi, A., Grasso, F. M., Merico, E., Guascito, M. R., & Contini, D. (2023). Concentration and size distribution of atmospheric particles in southern Italy during COVID-19 lockdown period. *Atmospheric Environment*, 295, 119559. <https://doi.org/10.1016/j.atmosenv.2022.119559>
- Delgado-Saborit, J. M., Guercio, V., Gowers, A. M., Shaddick, G., Fox, N. C., & Love, S. (2021). A critical review of the epidemiological evidence of effects of air pollution on dementia, cognitive function and cognitive decline in adult population. *Science of the Total Environment*, 757, 143734. <https://doi.org/10.1016/J.SCITOTENV.2020.143734>
- Deserti, M., Raffaelli, K., Ramponi, L., Carbonara, C., Agostini, C., Amorati, R., Arvani, B., Giovannini, G., Maccaferri, S., Poluzzi, V., et al. (2020). Report COVID-19-Studio Preliminare Degli Effetti Delle Misure COVID-19 Sulle Emissioni in Atmosfera e Sulla Qualità Dell'aria nel Bacino Padano-Giugno 2020; Technical Report, preAIR Project, 2020. [https://www.lifeprepare.eu/wp-content/uploads/2020/06/COVIDQA-Prepar-19Giugno2020\\_final.pdf](https://www.lifeprepare.eu/wp-content/uploads/2020/06/COVIDQA-Prepar-19Giugno2020_final.pdf)
- Dias, D., & Tchepel, O. (2018). Spatial and temporal dynamics in air pollution exposure assessment. *International Journal of Environmental Research and Public Health*, 15(3), 558. <https://doi.org/10.3390/ijerph15030558>
- Diémoz, H., Barnaba, F., Magri, T., Pession, G., Dionisi, D., Pittavino, S., Tombolato, I. K. F., Campanelli, M., Della Ceca, L. S., Hervo, M., Di Liberto, L., Ferrero, L., & Gobbi, G. P. (2019). Transport of Po Valley aerosol pollution to the northwestern Alps – Part 1: Phenomenology. *Atmospheric Chemistry and Physics*, 19, 3065–3095. <https://doi.org/10.5194/acp-19-3065-2019>
- Diémoz, H., Magri, T., Pession, G., Tarricone, C., Tombolato, I. K. F., Fasano, G., & Zublana, M. (2021). Air quality in the Italian Northwestern Alps during Year 2020: Assessment of the COVID-19 «lockdown effect» from multi-technique observations and models. *Atmosphere*, 12, 1006. <https://doi.org/10.3390/atmos12081006>
- Du, C., Liu, S., Yu, X., Li, X., Chen, C., Peng, Y., Dong, Y., Dong, Z., & Wang, F. (2013). Urban boundary layer height characteristics and relationship with particulate matter mass concentrations in Xi'an, Central China. *Aerosol and Air Quality Research*, 13, 1598–1607. <https://doi.org/10.4209/aaqr.2012.10.0274>
- Fan, H., Zhao, C., & Yang, Y. (2020). A comprehensive analysis of the spatio-temporal variation of urban air pollution in China during 2014–2018. *Atmospheric Environment*, 220, 117066. <https://doi.org/10.1016/j.atmosenv.2019.117066>
- Filigrana, P., Milando, C., Batterman, S., Levy, J. I., Mukherjee, B., & Adar, S. D. (2020). Spatiotemporal variations in traffic activity and their influence on air pollution levels in communities near highways. *Atmospheric Environment*, 242, 117758. <https://doi.org/10.1016/j.atmosenv.2020.117758>
- Finardi, S., Silibello, C., D'Allura, A., & Radice, P. (2014). Analysis of pollutants exchange between the Po Valley and the surrounding European region. *Urban Climate*, 10, 682–702. <https://doi.org/10.1016/j.uclim.2014.02.002>
- Galindo, N., Yubero, E., Nicolás, J. F., Varea, M., & Clemente, Á. (2018). Day-night variability of PM<sub>10</sub> components at a Mediterranean urban site during winter. *Air Quality, Atmosphere and Health*, 11, 1251–1258. <https://doi.org/10.1007/s11869-018-0627-8>
- Gilardoni, S., Massoli, P., Marinoni, A., Mazzoleni, C., Freedman, A., Lonati, G., De Iulii, S., & Gianelle, V. (2020). Spatial and temporal variability of carbonaceous aerosol absorption in the Po Valley. *Aerosol and Air Quality Research*, 20, 2624–2639. <https://doi.org/10.4209/aaqr.2020.03.0085>
- Giugliano, M., Lonati, G., Butelli, P., Romele, L., Tardivo, R., & Grosso, M. (2005). Fine particulate (PM<sub>2.5</sub>-PM<sub>1</sub>) at urban sites with different traffic exposure. *Atmospheric Environment*, 39, 2421–2431. <https://doi.org/10.1016/j.atmosenv.2004.06.050>
- Granella, F., Renna, S., & Aleluia Reis, L. (2024). The formation of secondary inorganic aerosols: A data-driven investigation of Lombardy's secondary inorganic aerosol problem. *Atmospheric Environment*, 327, 120480. <https://doi.org/10.1016/j.atmosenv.2024.120480>
- Heo, J.-B., Hopke, P. K., & Yi, S.-M. (2009). Source apportionment of PM<sub>2.5</sub> in Seoul. *Korea. Atmospheric Chemistry and Physics*, 9, 4957–4971. <https://doi.org/10.5194/acp-9-4957-2009>
- Hu, J., Wang, Y., Ying, Q., & Zhang, H. (2014). Spatial and temporal variability of PM<sub>2.5</sub> and PM<sub>10</sub> over the North China Plain and the Yangtze River Delta. *China. Atmospheric Environment*, 95, 598–609. <https://doi.org/10.1016/j.atmosenv.2014.07.019>
- Invernizzi, G., Ruprecht, A., Mazza, R., De Marco, C., Močnik, G., Sioutas, C., & Westerdaal, D. (2011). Measurement of black carbon concentration as an indicator of air quality

- benefits of traffic restriction policies within the Ecopass zone in Milan, Italy. *Atmospheric Environment*, 45, 3522–3527. <https://doi.org/10.1016/J.ATMOSENV.2011.04.008>
- Jain, S., Sharma, S. K., Vijayan, N., & Mandal, T. K. (2020). Seasonal characteristics of aerosols (PM<sub>25</sub> and PM<sub>10</sub>) and their source apportionment using PMF: A four year study over Delhi, India. *Environmental Pollution*, 262, 114337. <https://doi.org/10.1016/j.envpol.2020.114337>
- Juginović, A., Vuković, M., Aranza, I., & Biloš, V. (2011). Health impacts of air pollution exposure from 1990 to 2019 in 43 European countries. *Scientific Reports*, 11, 22516. <https://doi.org/10.1038/s41598-021-01802-5>
- Jung, J., Souri, A. H., Wong, D. C., Lee, S., Jeon, W., Kim, J., & Choi, Y. (2019). The impact of the direct effect of aerosols on meteorology and air quality using aerosol optical depth assimilation during the KORUS-AQ campaign. *JGR Atmospheres*, 124, 8303–8319. <https://doi.org/10.1029/2019JD030641>
- Kim, E., Hopke, P. K., & Edgerton, E. S. (2003). Source identification of Atlanta aerosol by positive matrix factorization. *Journal of the Air & Waste Management Association*, 53, 731–739. <https://doi.org/10.1080/10473289.2003.10466209>
- Kuehn, B. M. (2014). WHO: More than 7 million air pollution deaths each year. *JAMA*, 311, 1486. <https://doi.org/10.1001/jama.2014.4031>
- Kuerban, M., Waili, Y., Fan, F., Liu, Y., Qin, W., Dore, A. J., Peng, J., Xu, W., & Zhang, F. (2020). Spatio-temporal patterns of air pollution in China from 2015 to 2018 and implications for health risks. *Environmental Pollution*, 258, 113659. <https://doi.org/10.1016/j.envpol.2019.113659>
- Lestari, P., Oskouie, A. K., & Noll, K. E. (2003). Size distribution and dry deposition of particulate mass, sulfate and nitrate in an urban area. *Atmospheric Environment*, 37, 2507–2516. [https://doi.org/10.1016/S1352-2310\(03\)00151-1](https://doi.org/10.1016/S1352-2310(03)00151-1)
- Li, R., Cui, L., Li, J., Zhao, A., Fu, H., Wu, Y., Zhang, L., Kong, L., & Chen, J. (2017a). Spatial and temporal variation of particulate matter and gaseous pollutants in China during 2014–2016. *Atmospheric Environment*, 161, 235–246. <https://doi.org/10.1016/J.ATMOSENV.2017.05.008>
- Li, X., Ma, Y., Wang, Y., Liu, N., & Hong, Y. (2017b). Temporal and spatial analyses of particulate matter (PM<sub>10</sub> and PM<sub>2.5</sub>) and its relationship with meteorological parameters over an urban city in northeast China. *Atmospheric Research*, 198, 185–193. <https://doi.org/10.1016/j.atmosres.2017.08.023>
- Li, C., Huang, Y., Guo, H., Wu, G., Wang, Y., Li, W., & Cui, L. (2019). The concentrations and removal effects of PM<sub>10</sub> and PM<sub>2.5</sub> on a Wetland in Beijing. *Sustainability*, 11(5), 1312. <https://doi.org/10.3390/su11051312>
- Lipfert, F. W. (2018). Long-term associations of morbidity with air pollution: A catalog and synthesis. *Journal of the Air & Waste Management Association*, 68, 12–28. <https://doi.org/10.1080/10962247.2017.1349010>
- Liu, S., Tian, H., Luo, L., Bai, X., Zhu, C., Lin, S., Zhao, S., Zhang, K., Hao, J., Guo, Z., & Lv, Y. (2022). Health impacts and spatiotemporal variations of fine particulate and its typical toxic constituents in five urban agglomerations of China. *Science of the Total Environment*, 806, 151459. <https://doi.org/10.1016/J.SCITOTENV.2021.151459>
- Lonati, G., Giugliano, M., & Cernuschi, S. (2006). The role of traffic emissions from weekends' and weekdays' fine PM data in Milan. *Atmospheric Environment*, 40, 5998–6011. <https://doi.org/10.1016/J.ATMOSENV.2005.12.033>
- Lonati, G., Crippa, M., Gianelle, V., & Van Dingenen, R. (2011). Daily patterns of the multi-modal structure of the particle number size distribution in Milan, Italy. *Atmospheric Environment*, 45, 2434–2442. <https://doi.org/10.1016/j.atmosenv.2011.02.003>
- Lonati, G., & Trentini, A. (2019). Particle number concentrations in the Po Valley (Northern Italy) in wintertime: Comparison between urban and rural sites (pp. 23–27). <https://re.public.polimi.it/retrieve/e0c31c0f-293d-4599-e053-1705fe0aef77/WCAC2019-Proceedings%20Lonati%20Trentini.pdf>
- Ma, X., & Jia, H. (2016). Particulate matter and gaseous pollutants in three megacities over China: Situation and implication. *Atmospheric Environment*, 140, 476–494. <https://doi.org/10.1016/j.atmosenv.2016.06.008>
- Maurizi, A., Russo, F., & Tampieri, F. (2013). Local vs. external contribution to the budget of pollutants in the Po Valley (Italy) hot spot. *Science of the Total Environment*, 458–460, 459–465. <https://doi.org/10.1016/j.scitotenv.2013.04.026>
- Mehmood, U., Azhar, A., Qayyum, F., Nawaz, H., Tariq, S., & Haq, Z. U. (2021). Air pollution and hospitalization in megacities: Empirical evidence from Pakistan. *Environmental Science and Pollution Research*, 28, 51384–51390. <https://doi.org/10.1007/s11356-021-14158-0>
- Michetti, M., Gualtieri, M., Anav, A., Adani, M., Benassi, B., Dalmastrì, C., D'Elia, I., Piersanti, A., Sannino, G., Zanini, G., & Uccelli, R. (2022). Climate change and air pollution: Translating their interplay into present and future mortality risk for Rome and Milan municipalities. *Science of the Total Environment*, 830, 154680. <https://doi.org/10.1016/J.SCITOTENV.2022.154680>
- ONU. (2015). *Transforming our world: The 2030 agenda for sustainable development* (pp. 12–14). <https://sustainabledevelopment.un.org/content/documents/21252030%20Agenda%20for%20Sustainable%20Development%20web.pdf>
- Ouyang, W., Guo, B., Cai, G., Li, Q., Han, S., Liu, B., & Liu, X. (2015). The washing effect of precipitation on particulate matter and the pollution dynamics of rainwater in downtown Beijing. *Science of the Total Environment*, 505, 306–314. <https://doi.org/10.1016/j.scitotenv.2014.09.062>
- Pecorari, E., Squizzato, S., Masiol, M., Radice, P., Pavoni, B., & Rampazzo, G. (2013). Using a photochemical model to assess the horizontal, vertical and time distribution of PM<sub>2.5</sub> in a complex area: Relationships between the regional and local sources and the meteorological conditions. *Science of the Total Environment*, 443, 681–691. <https://doi.org/10.1016/J.SCITOTENV.2012.11.047>
- Pernigotti, D., Georgieva, E., Thunis, P., & Bessagnet, B. (2012). Impact of meteorology on air quality modeling over the Po Valley in northern Italy. *Atmospheric Environment*, 51, 303–310. <https://doi.org/10.1016/J.ATMOS.ENV.2011.12.059>

- Perrone, M. G., Larsen, B. R., Ferrero, L., Sangiorgi, G., De Gennaro, G., Udisti, R., Zangrando, R., Gambaro, A., & Bolzacchini, E. (2012). Sources of high PM<sub>2.5</sub> concentrations in Milan, Northern Italy: Molecular marker data and CMB modelling. *Science of the Total Environment*, *414*, 343–355. <https://doi.org/10.1016/j.scitotenv.2011.11.026>
- Pognant, F., Bo, M., Nguyen, C. V., Salizzoni, P., & Clerico, M. (2017). Modelling and evaluation of emission scenarios deriving from wood biomass boilers in alpine valley. In *HARMO 2017 - 18th international conference on harmonisation within atmospheric dispersion modelling for regulatory purposes, proceedings* (pp. 278–282). Conference proceeding. [https://harmo.org/Conferences/Proceedings/\\_Bologna/publishedSections/H18-154-Pognant.pdf](https://harmo.org/Conferences/Proceedings/_Bologna/publishedSections/H18-154-Pognant.pdf)
- Qayyum, F., Mehmood, U., Tariq, S., Haq, Z. U., & Nawaz, H. (2021). Particulate matter (PM<sub>2.5</sub>) and diseases: An autoregressive distributed lag (ARDL) technique. *Environmental Science and Pollution Research*, *28*, 67511–67518. <https://doi.org/10.1007/s11356-021-15178-6>
- Rai, P., Chakraborty, A., Mandariya, A. K., & Gupta, T. (2016). Composition and source apportionment of PM<sub>1</sub> at urban site Kanpur in India using PMF coupled with CBPF. *Atmospheric Research*, *178–179*, 506–520. <https://doi.org/10.1016/j.atmosres.2016.04.015>
- Ramanathan, V., & Carmichael, G. (2008). Global and regional climate changes due to black carbon. *Nature Geoscience*, *1*, 221–227. <https://doi.org/10.1038/ngeo156>
- Squizzato, S., & Masiol, M. (2015). Application of meteorology-based methods to determine local and external contributions to particulate matter pollution: A case study in Venice (Italy). *Atmospheric Environment*, *119*, 69–81. <https://doi.org/10.1016/j.atmosenv.2015.08.026>
- Squizzato, S., Cazzaro, M., Innocente, E., Visin, F., Hopke, P. K., & Rampazzo, G. (2017). Urban air quality in a mid-size city — PM<sub>2.5</sub> composition, sources and identification of impact areas: From local to long range contributions. *Atmospheric Research*, *186*, 51–62. <https://doi.org/10.1016/j.atmosres.2016.11.011>
- Steffen, W., Richardson, K., Rockström, J., Cornell, S. E., Fetzer, I., Bennett, E. M., Biggs, R., Carpenter, S. R., de Vries, W., de Wit, C. A., Folke, C., Gerten, D., Heinke, J., Mace, G. M., Persson, L. M., Ramanathan, V., Reyers, B., & Sörlin, S. (2015). Planetary boundaries: Guiding human development on a changing planet. *Science*, *347*. <https://doi.org/10.1126/science.1259855>
- Su, T., Li, Z., & Kahn, R. (2018). Relationships between the planetary boundary layer height and surface pollutants derived from lidar observations over China: Regional pattern and influencing factors. *Atmospheric Chemistry and Physics*, *18*, 15921–15935. <https://doi.org/10.5194/acp-18-15921-2018>
- Sullivan, A. P., Hodas, N., Turpin, B. J., Skog, K., Keutsch, F. N., Gilardoni, S., Paglione, M., Rinaldi, M., Decesari, S., Facchini, M. C., Poulain, L., Herrmann, H., Wiedensohler, A., Nemitz, E., Twigg, M. M., & Collett, J. L., Jr. (2016). Evidence for ambient dark aqueous SOA formation in the Po Valley, Italy. *Atmospheric Chemistry and Physics*, *16*, 8095–8108. <https://doi.org/10.5194/acp-16-8095-2016>
- Tian, D., Fan, J., Jin, H., Mao, H., Geng, D., Hou, S., et al. (2020). Characteristic and spatiotemporal variation of air pollution in Northern China based on correlation analysis and clustering analysis of five air pollutants. *Journal of Geophysical Research: Atmospheres*, *125*, e2019JD031931. <https://doi.org/10.1029/2019JD031931>
- Tiwari, S., Bisht, D. S., Srivastava, A. K., Pipal, A. S., Taneja, A., Srivastava, M. K., & Attri, S. D. (2014). Variability in atmospheric particulates and meteorological effects on their mass concentrations over Delhi, India. *Atmospheric Research*, *145–146*, 45–56. <https://doi.org/10.1016/j.atmosres.2014.03.027>
- Tiwari, S., Dumka, U. C., Gautam, A. S., Kaskaoutis, D. G., Srivastava, A. K., Bisht, D. S., Chakrabarty, R. K., Sumlin, B. J., & Solmon, F. (2017). Assessment of PM<sub>2.5</sub> and PM<sub>10</sub> over Guwahati in Brahmaputra River Valley: Temporal evolution, source apportionment and meteorological dependence. *Atmospheric Pollution Research*, *8*, 13–28. <https://doi.org/10.1016/j.apr.2016.07.008>
- Tositti, L., Brattich, E., Masiol, M., Baldacci, D., Ceccato, D., Parmeggiani, S., Stracquadanio, M., & Zappoli, S. (2014). Source apportionment of particulate matter in a large city of southeastern Po Valley (Bologna, Italy). *Environmental Science and Pollution Research*, *21*, 872–890. <https://doi.org/10.1007/s11356-013-1911-7>
- Trivelli, L., Borrelli, P., Cadum, E., Pisoni, E., & Villani, S. (2021). Spatial-temporal modelling of disease risk accounting for PM<sub>2.5</sub> exposure in the province of Pavia: An area of the Po Valley. *International Journal of Environmental Research and Public Health*, *18*, 658. <https://doi.org/10.3390/ijerph18020658>
- UN. (2018). The world's cities in 2018. <https://digitallibrary.un.org/record/3799524?v=pdf>
- Ur Rehman, Z., Tariq, S., Ul Haq, Z., & Khan, M. (2024). Impact of meteorological parameters on aerosol optical depth and particulate matter in Lahore. *Acta Geophysica*. <https://doi.org/10.1007/s11600-024-01291-w>
- Uria-Tellaetxe, I., & Carslaw, D. C. (2014). Conditional bivariate probability function for source identification. *Environmental Modelling and Software*, *59*, 1–9. <https://doi.org/10.1016/j.envsoft.2014.05.002>
- Wang, D., Zhou, B., Fu, Q., Zhao, Q., Zhang, Q., Chen, J., Yang, X., Duan, Y., & Li, J. (2016). Intense secondary aerosol formation due to strong atmospheric photochemical reactions in summer: Observations at a rural site in eastern Yangtze River Delta of China. *Science of the Total Environment*, *571*, 1454–1466. <https://doi.org/10.1016/J.SCITOTENV.2016.06.212>
- Xu, G., Jiao, L., Zhang, B., Zhao, S., Yuan, M., Gu, Y., Liu, J., & Tang, X. (2017). Spatial and temporal variability of the PM<sub>2.5</sub>/PM<sub>10</sub> ratio in Wuhan, Central China. *Aerosol and Air Quality Research*, *17*, 741–751. <https://doi.org/10.4209/aaqr.2016.09.0406>
- Xue, W., Xue, J., Shirmohammadi, F., Sioutas, C., Lolinco, A., Hasson, A., & Kleeman, M. J. (2020). Day-of-week patterns for ultrafine particulate matter components at four sites in California. *Atmospheric Environment*, *222*, 117088. <https://doi.org/10.1016/j.atmosenv.2019.117088>
- Yao, Y., Wang, K., & Xiang, H. (2022). Association between cognitive function and ambient particulate matters in middle-aged and elderly Chinese adults: Evidence from the China Health and Retirement Longitudinal Study (CHARLS). *Science of the Total Environment*, *828*, 154297. <https://doi.org/10.1016/J.SCITOTENV.2022.154297>

- Zhang, S., Wu, Y., Huang, R., Wang, J., Yan, H., Zheng, Y., & Hao, J. (2016). High-resolution simulation of link-level vehicle emissions and concentrations for air pollutants in a traffic-populated eastern Asian city. *Atmospheric Chemistry and Physics*, 16, 9965–9981. <https://doi.org/10.5194/acp-16-9965-2016>
- Zhang, L., Zhang, Z., Feng, C., Tian, M., & Gao, Y. (2021). Impact of various vegetation configurations on traffic fine particle pollutants in a street canyon for different wind regimes. *Science of the Total Environment*, 789, 147960. <https://doi.org/10.1016/J.SCITOTENV.2021.147960>
- Zhao, S., Yu, Y., Yin, D., Qin, D., He, J., & Dong, L. (2018). Spatial patterns and temporal variations of six criteria air pollutants during 2015 to 2017 in the city clusters of Sichuan Basin, China. *Science of the Total Environment*, 624, 540–557. <https://doi.org/10.1016/j.scitotenv.2017.12.172>

**Publisher's Note** Springer Nature remains neutral with regard to jurisdictional claims in published maps and institutional affiliations.